Spin and charge dynamics in the hole-doped one-dimensional-chain–ladder composite material $Sr_{14}Cu_{24}O_{41}$: Cu NMR/NQR studies

Masashi Takigawa*
IBM Thomas J. Watson Research Center, P.O. Box 218, Yorktown Heights, New York 10598

Naoki Motoyama, Hiroshi Eisaki, and Shinichi Uchida
Department of Superconductivity, University of Tokyo, Bunkyo-ku, Tokyo 113, Japan
(Received 11 June 1997)

Comprehensive ^{63,65}Cu NMR/NQR measurements have been performed on single crystals of $Sr_{14}Cu_{24}O_{41}$, a hole-doped material containing alternating layers of one-dimensional CuO_2 chains and Cu_2O_3 ladders. While the ladder sites show a unique resonance, two distinct resonance spectra are obtained for the chain sites. They are assigned to the magnetic Cu sites with spin-1/2 and the nonmagnetic Cu sites, which form the Zhang-Rice (ZR) singlet with holes on the oxygen sites. The NMR spectrum at the ZR chain sites shows sharp multipeak structure at low temperatures, indicating a long period of superstructure. The structure becomes obscure and peaks merge into a single broad line with increasing temperature due to thermally induced disorder or motion. A giant oscillation of the spin-echo intensity was observed at the magnetic chain sites as a function of the time separation between $\pi/2$ and π rf pulses. This is well explained if these sites form spin-singlet dimers, which interact very weakly with each other. The nuclear spin-lattice relaxation rate $(1/T_1)$ at both chain sites shows an activated temperature dependence below $T=50$ K with a gap of 125 K, corresponding to the singlet-triplet splitting of the dimers. The ZR chain sites show an anomalous increase of $1/T_1$ above 200 K. The ladder Cu sites also show an activated temperature dependence of $1/T_1$ with a gap of 650 K above 200 K, indicating a spin-gap in the ladders. However, $1/T_1$ at the ladder sites measured by zero-field NQR is dominantly caused by fluctuations of the electric-field gradient (EFG) in the temperature range 30–150 K and shows a peak near $T=100$ K. This is most likely caused by slow motion of doped holes and/or lattice distortion. The inverse correlation time of the EFG fluctuations is estimated using a simple model of motional effects. It shows an activated temperature dependence with a gap of 230 K, which is an order of magnitude smaller than the activation energy for the electrical conductivity (2200 K). [S0163-1829(98)05402-2]

I. INTRODUCTION

Although the study of one-dimensional (1D) magnetism has very long history, recent discovery of various quasi-1D quantum antiferromagnets and progress in analytic and numerical theories have significantly advanced this field. A spin-1/2 Heisenberg chain with a nearest-neighbor exchange shows quantum critical behavior[1] that both the antiferromagnetic correlation length and the characteristic time scale of spin fluctuations diverge as $1/T$ at low temperatures, even though no long-range order is achieved at $T=0$. This behavior has been supported by recent nuclear magnetic resonance (NMR) experiments[2] on Sr_2CuO_3. A weak perturbation can change such a critical ground state into either a Néel ordered state or a more disordered state. For example, weak interchain coupling induces 3D antiferromagentic order with a small ordered moment,[3] while coupling to phonons induces a spin-Peierls transition into a dimerized singlet ground state with an energy gap in the spin excitations spectrum.

Coupling two spin-1/2 Heisenberg chains to form a ladder also leads to a singlet ground state with a spin-gap and a finite correlation length at $T=0$. This was predicted theoretically[4–8] and confirmed by subsequent experiments on compounds with ladder structure such as $SrCu_2O_3$ (Ref. 9) and $(VO)_2P_2O_7$.[10] The existence of a spin gap is obvious in the limit that the interchain exchange along the rung is much larger than the intrachain exchange along the leg,[4,5] since the ground state is then simply a collection of singlets along the rung. For a general ratio of the two exchange constants, the ground state is a resonating valence bond state,[6,8] in which singlet pairs are resonating along the rung and along the leg. A remarkable theoretical prediction was made[4,5,11,12] that mobile holes doped into such spin ladders would be bound in pairs, leading either to superconducting condensation or a charge-ordered ground state. Intuitively, the hole pairing is due to the gain in exchange energy when two holes are bound closely so that all spins can still make pairs, compared to the case when they are far apart and, therefore, two singlet pairs have to be broken. Thus the recent discovery of superconductivity in $Sr_{14-x}Ca_xCu_{24}O_{41}$,[13] which includes the ladder structure as its subunit, has raised great interest in this material, which remained largely unexplored until recently since the early days of high-T_c activities.[14,15]

The structure of $Sr_{14}Cu_{24}O_{41}$ shown in Fig. 1 has the alternating stack of Sr-CuO_2–Sr-Cu_2O_3 layers.[15] The CuO_2 subunit contains linear chains in which nearest-neighbor Cu ions are coupled by two Cu-O-Cu bonds with a nearly 90° bond angle. This structure is similar to the spin-Peierls compound $CuGeO_3$.[16] The Cu_2O_3 subunit contains ladders in which Cu ions are coupled via nearly 180° Cu-O-Cu bonds. The ladders are coupled by 90° Cu-O-Cu bonds. The interladder exchange is frustrating and expected

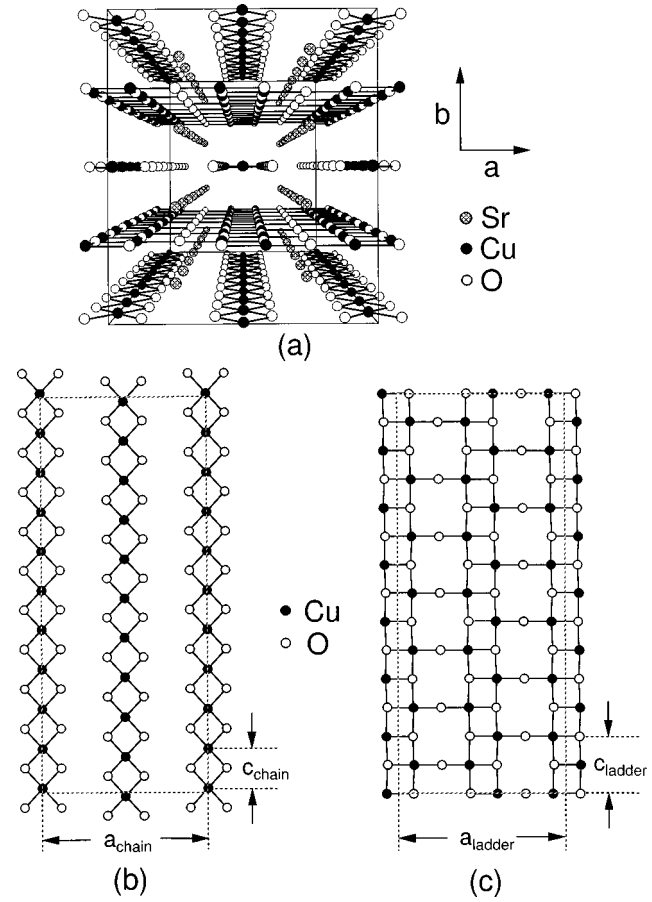

FIG. 1. The crystal structure of $Sr_{14}Cu_{24}O_{41}$. (b) and (c) show the CuO_2 chain and Cu_2O_3 ladder subunit, respectively.

to be much weaker than the intraladder exchange. This subunit has the same structure as the two-leg spin-ladder material $SrCu_2O_3$,[17,9] for which the presence of a gap has been established. The Cu-Cu distance in these two subunits are incommensurate but satisfy the approximate relation $10 \times c_{chain} \simeq 7 \times c_{ladder}$.[15] A significant feature of this material is the average Cu valence of +2.25, i.e., six holes per formula unit are already doped without substitution. Of course the average valence changes if there is oxygen nonstoichiometry or cation deficiencies. The electrical resistivity is highly anisotropic and is of the order of $10^{-3}\Omega$ cm along the most conducting c axis at room temperature.[18] It shows a semiconducting temperature dependence with an activation energy of 2200 K, therefore, the holes must be localized at low temperatures.

The magnetic properties of $Sr_{14}Cu_{24}O_{41}$ have been studied by susceptibility (χ),[19,20,18] NMR/NQR (nuclear quadrupole resonance),[21–23] electron-spin resonance (ESR),[19] and neutron-scattering experiments.[24,25] In Fig. 2 is shown the temperature dependence of χ along the a direction measured by Motoyama *et al.*[18] It shows a maximum at 80 K and an activated behavior is revealed at lower temperatures after subtracting the Curie term. Carter *et al.*[20] argued that the susceptibility from Cu_2O_3 ladders should be negligibly small compared with the measured χ below 200 K, if one assumes that the the former can be approximated by the susceptibility of the isostructural $SrCu_2O_3$ that has an excitation gap of 420 K.[9] A large activation gap of 500–700 K has been indeed observed by the NMR relaxation rate at the ladder Cu sites[21–23] and the neutron-scattering spectrum[25] was found to be consistent with a gap of 35 meV for the ladder. Thus the susceptibility data indicates that the ground state of CuO_2 chains is also a singlet with a spin gap. The decrease of the ESR intensity at low temperatures[19] also indicates a singlet ground state.

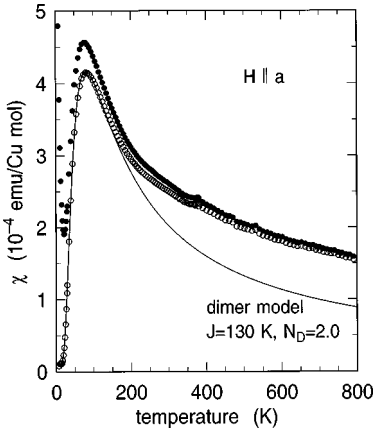

FIG. 2. Temperature dependence of the magnetic susceptibility along the a direction measured by Motoyama *et al.* (Ref. 18). The solid dots represent the raw data and the open circles are obtained by subtracting the Curie term. The line indicates the result of the dimer model as described in the text.

Matsuda and Katsumata[19] and Carter *et al.*[20] found that a simple dimer model (an isolated pair of antiferromagnetically coupled spin-1/2) gives a good fit to the low-temperature part of χ. The solid line in Fig. 2 shows the result of the dimer model $\chi = 2N_D(g\mu_B)^2/k_BT[3 + \exp(J/k_BT)]$ with the number of dimers $N_D = 2.0$ per formula unit ($g = 2.05$ along the a direction[19]) and the intradimer exchange $J = 130$ K. The NQR relaxation rate at the chain Cu sites[22,23] also revealed an activation energy of about 140 K. The deviation of χ from the dimer model at high temperatures can be attributed to the contribution from the ladders. Although there are ten chain Cu atoms in a formula unit, the susceptibility data implies that only four of them contribute to χ. A natural explanation is that each hole doped into the chains occupies a linear combination of $2p$ orbitals on the four oxygen sites surrounding a Cu cite and form the Zhang-Rice (ZR) singlet[26] with the central Cu spin, thereby reduces the number of active Cu spins. The dimerization has been supported also by neutron-scattering experiments by Matsuda *et al.*,[24] who observed strong inelastic peaks from the chains in the energy range 9–13 meV with weak dispersion.

The optical reflectivity in $Sr_{14}Cu_{24}O_{41}$ (Ref. 27) shows a plasma edge at 0.5 eV. The low energy (below 1.2 eV) spectral weight of the optical conductivity increases as Sr is replaced with Ca, indicating the hole redistribution from chains to ladders. The dc resistivity also becomes more metallic with Ca substitution,[28,20,18] until finally superconductivity sets in[13] for $Sr_{0.4}Ca_{13.6}Cu_{24}O_{41}$ below $T_c = 12$ K under a pressure of 3 GPa.

In this paper, we report results of comprehensive NMR/NQR experiments at both the ladder and the chain Cu sites in $Sr_{14}Cu_{24}O_{41}$. Compared with the previous NMR/NQR results[21–23] on powder samples, which mostly focused on

establishing spin gaps at both Cu sites, our results on single crystals revealed rich spectral feature and unexpected relaxation phenomena. While the nuclear spin-lattice relaxation rate at the ladder sites measured by NQR at zero field shows an activated temperature dependence above $T=200$ K with an activation energy of 650 K, it shows a minimum at $T=150$ K and a broad maximum near $T=100$ K. The nuclear relaxation is dominantly caused by fluctuations of the local electric field gradient via the nuclear quadrupole coupling in the temperature range 30–150 K. The correlation time for charge fluctuations is estimated. Two distinct NMR spectra are observed for the chain Cu sites, which are identified as the dimer and the ZR singlet sites. The spectrum at the ZR singlet sites shows a sharp structure with many peaks at low temperatures, indicating the existence of microscopically inequivalent sites due to superstructure. These peaks get broadened and eventually merge into a single broad line at high temperatures, indicating that the site distinction becomes obscure due to thermally induced disorder or motion. A giant oscillation of the spin-echo intensity is observed at the dimer chain sites as a function of the time separation between $\pi/2$ and π rf pulses. This is explained by nuclear spin-spin coupling between two sites within a dimer, which is well separated from other dimers. Models of charge order and dimerization in the chains are presented.

In Sec. II we describe the experimental procedure and a brief summary of how to obtain the shift, the quadrupole splitting, the spin-lattice, and the spin-spin relaxation rates from NMR/NQR measurements in spin systems. The NMR/NQR results on the ladder (chain) Cu sites are presented and analyzed in Sec. III A (Sec. III B). The implication of the results on the spin and charge dynamics in this material is discussed in Sec. IV, followed by a summary in Sec. V.

II. EXPERIMENTAL PROCEDURE

Single crystals of $Sr_{14}Cu_{24}O_{41}$ were grown by the traveling-solvent floating-zone method[18] using a infrared furnace in an oxygen atmosphere at 3 bars. Two single crystals were used in these studies. The crystal used in high-field NMR measurements has the dimension $4\times5\times2$ mm^3. A somewhat larger piece ($4\times8\times3$ mm^3) was used for zero-field NQR measurements.

Since the results presented in the next section are obtained from a wide variety of NMR/NQR measurements and are related to many different aspects of resonance phenomena, it will be useful to summarize here the basic formulas used to obtain these results in a systematic way.[29,30] We consider explicitly two Cu isotopes (^{63}Cu and ^{65}Cu) with nuclear spin $I=3/2$ in a magnetic insulator. The Hamiltonian acting on a nuclear spin at ith sites $\mathbf{I}^i$ can be written as

$$\mathcal{H}=\gamma_n\hbar H_0 I_z^i+\sum_j \mathbf{I}^i\cdot\mathbf{A}^{i-j}\cdot\mathbf{S}^j+2\mu_B\gamma_n\hbar\langle r^{-3}\rangle\mathbf{I}^i\cdot\mathbf{L}^i + \sum_{\alpha\beta} V_{\alpha\beta}^i Q_{\alpha\beta}^i, \tag{1}$$

where the first term is the Zeeman energy due to external field along the z direction (γ_n is the nuclear gyromagnetic ratio), the second and the third terms are the magnetic hyperfine interactions with electron spin and orbital moments, respectively, and the final term is the quadrupole interaction between electric-field gradient (EFG) at the nuclear position $V_{\alpha\beta}=\partial^2V/\partial x_\alpha\partial x_\beta$ and nuclear quadrupole moments $Q_{\alpha\beta}=eQ/\{6I(2I-1)\}\{3/2(I_\alpha I_\beta+I_\beta I_\alpha)-\delta_{\alpha\beta}I(I+1)\}$. Note that the spin hyperfine interaction generally has a finite range. It is usually sufficient to consider the on-site and the nearest-neighbor coupling, $\mathbf{A}^0$ and $\mathbf{A}^1$. The Hamiltonian can be divided into the static (time averaged) and the fluctuating parts, $\mathcal{H}=\mathcal{H}_{\rm st}+\mathcal{H}_{\rm fl}$, where

$$\mathcal{H}_{\rm st}=\gamma_n\hbar H_0 I_z^i+\sum_j \mathbf{I}^i\cdot\mathbf{A}^{i-j}\cdot\langle\mathbf{S}^j\rangle+2\mu_B\gamma_n\hbar\langle r^{-3}\rangle\mathbf{I}^i\cdot\langle\mathbf{L}^i\rangle + \sum_{\alpha\beta}\langle V_{\alpha\beta}^i\rangle Q_{\alpha\beta}^i$$

$$=\gamma_n\hbar H_0(1+K_z)I_z^i+\sum_{\alpha\beta}\langle V_{\alpha\beta}^i\rangle Q_{\alpha\beta}^i, \tag{2a}$$

$$\mathcal{H}_{\rm fl}=\sum_j \mathbf{I}^i\cdot\mathbf{A}^{i-j}\cdot\delta\mathbf{S}^j+\sum_{\alpha\beta}\delta V_{\alpha\beta}^i Q_{\alpha\beta}^i, \tag{2b}$$

with

$$K_z=K_{z,\rm spin}+K_{z,\rm orb}$$

$$K_{z,\rm spin}=\sum_j \frac{A_{zz}^{i-j}\chi_{z,\rm spin}}{g\mu_B\gamma_n\hbar},\quad K_{z,\rm orb}=2\langle r^{-3}\rangle\chi_{z,\rm orb}, \tag{3}$$

where $\chi_{\rm spin}$ and $\chi_{\rm orb}$ are the spin and the (van Vleck) orbital susceptibility. The term containing $\delta\mathbf{L}$ has been dropped since it is unimportant for Cu^{2+} with a nondegenerate orbital state.

We first discuss the static part Eq. (2a), which determines the basic feature of NMR/NQR spectra. If the nuclear position has a cubic point symmetry, $\langle V_{\alpha\beta}\rangle=0$ and the first term gives equally spaced nuclear-spin energy levels $E_m=\gamma_n\hbar H_0(1+K_z)m$ $(m=I_z)$. Since the transitions $I_z=m\leftrightarrow m\pm1$ are observed in NMR, there is a single resonance line at a frequency $(1+K^z)\nu_0$, where $\nu_0=\gamma_nH_0/2\pi$ is the resonance frequency in a diamagnetic substance. Hence K_z is called the magnetic shift. In a noncubic environment, the second term also leads to the splitting of nuclear spin levels and resonance between them can be observed even when $H_0=0$ (nuclear quadrupole resonance, NQR). For $I=3/2$, there are two doubly degenerate levels, giving rise to a single NQR line. When both H_0 and $\langle V_{\alpha\beta}\rangle$ are not zero, we consider the case relevant to our experiments that the first term in Eq. (2a) is much larger than the second term so that the latter can be treated by a perturbation theory up to second order. We assume that the magnetic field is along one of the principal axes of the EFG tensor so that $\langle V_{\alpha\beta}\rangle=0$ for $\alpha\neq\beta$. Since in $Sr_{14}Cu_{24}O_{41}$, the crystalline a, b, and c axes are approximately the principal axes of both EFG and the hyperfine coupling tensor, this condition will be met when the field is applied along one of the crystalline axes. The resonance frequency for the $I_z=m\leftrightarrow m-1$ transition is given as

$$\nu_m=(1+K_z)\nu_0-\nu_z(m-1/2)+\delta_{m,1/2}\frac{(\nu_x-\nu_y)^2}{12(1+K_z)\nu_0}, \quad (4)$$

where $\nu_\alpha=\langle V_{\alpha\alpha}\rangle(eQ/2h)$. There are three resonance lines for $I=3/2$. The central line ($m=1/2$) is unshifted by the first-order quadrupole effect but shifted by the second-order effect. The satellite lines ($m=3/2,-1/2$) are shifted only by the first-order effect. Measurement of $\nu_{3/2}$ and $\nu_{-1/2}$ determines K_z and $|\nu_z|$. One can also determine K_z and $|\nu_x-\nu_y|$ by measuring $\nu_{1/2}$ for more than two different values of ν_0 (H_0). Since K_z determined in both ways should be identical, one can identify which central and satellite lines belong to the same site when there are many different sites. Another important fact is that, since $\Sigma_\alpha\nu_\alpha=0$, all three values of $|\nu_\alpha|$ ($\alpha=x$, y, and z) can be determined from measurements for only one direction of field. This enables us to identify which sets of quadrupole split lines for different field orientation belong to the same sites. The NQR frequency at zero field is then equal to $\sqrt{2/3}(\nu_x^2+\nu_y^2+\nu_z^2)^{1/2}$.

In our experiments, the NQR spectra at zero magnetic field were obtained by adding Fourier-transformed spectra of spin-echo signal taken at discrete frequencies, whose spacing is smaller than the spectrometer band width which is typically 200 kHz. The NMR spectra at high magnetic field were obtained by recording the integrated intensity of the spin-echo signal by a boxcar averager while sweeping the magnetic field, instead of changing the frequency at a fixed magnetic field.

Let us turn to the fluctuating part Eq. (2b). Such a time-dependent perturbation causes transitions between different nuclear-spin levels and leads to the spin-lattice relaxation phenomena. In our experiments, the spin-lattice relaxation rate ($1/T_1$) was measured by the inversion recovery method. First a π pulse is applied to invert the populations of the two levels, between which the resonance is being observed. The recovery of the populations toward the thermal equilibrium is monitored by the intensity of the spin-echo signal at a time t after the π pulse. In NQR experiments, where there is only one resonance line, the spin-echo intensity follows a single exponential function

$$I(t)=I_\infty-\{I_\infty-I(0)\}\exp(-t/T_{1,\mathrm{NQR}}), \quad (5)$$

where $1/T_{1,\mathrm{NQR}}$ is twice the transition probability between the nuclear-spin levels. Since usually there is no correlation between the two terms in Eq. (2b), both terms contribute to $1/T_{1,\mathrm{NQR}}$ additively,

$$1/T_{1,\mathrm{NQR}}=(1/T_1)_M+(1/T_1)_Q, \quad (6)$$

where $(1/T_1)_M$ is the magnetic relaxation rate due to spin fluctuations and $(1/T_1)_Q$ is the quadrupole relaxation rate due to phonons and charge fluctuations. These two contributions can be separated experimentally by measuring $1/T_1$ for the two isotopes with sufficient accuracy, since $(1/T_1)_M \propto\gamma_n^2$ and $(1/T_1)_Q\propto Q^2$ and the isotopic ratio of these moments are different, $(^{65}\gamma_n/^{63}\gamma_n)^2=1.148$, $(^{65}Q/^{63}Q)^2=0.856$. In high-field NMR experiments, the recovery of the spin-echo intensity depends on which transition is being observed. If the relaxation is purely magnetic, the recovery curve is given as[31]

$$I(t)=I_\infty-\{I_\infty-I(0)\}\{0.9\exp(-6t/T_1)+0.1\exp(-t/T_1)\} \quad (7a)$$

for the central line and

$$I(t)=I_\infty-\{I_\infty-I(0)\}\{0.4\exp(-6t/T_1)+0.5\exp(-3t/T_1)+0.1\exp(-t/T_1)\} \quad (7b)$$

for the satellite lines and $1/T_1$ is related to the spin-correlation function by[32]

$$1/T_1=(1/2\hbar^2)\sum_{\alpha=x,y}\sum_{\mathbf{q}}|A_\alpha(\mathbf{q})|^2\int_{-\infty}^{\infty}\exp(-i\omega_0 t)\times\langle\delta S_\alpha(\mathbf{q},t)\,\delta S_\alpha(-\mathbf{q},0)\rangle dt, \quad (8)$$

where $\mathbf{A}(\mathbf{q})=\Sigma_j\mathbf{A}^{i-j}\exp(i\mathbf{R}^{i-j}\cdot\mathbf{q})$, $\delta\mathbf{S}(\mathbf{q})=(1/\sqrt{N})\Sigma_j\delta\mathbf{S}^j\exp(i\mathbf{R}^j\cdot\mathbf{q})$, ω_0 is the NMR frequency and $\mathbf{A}$ is assumed to be diagonal. Similarly, the quadrupole relaxation is related to the correlation function of EFG. However, since it involves two types of transitions, one with $\Delta I_z=1$ and the other with $\Delta I_z=2$, there is no unique expression for quadrupole relaxation such as Eqs. (7) and (8).

So far we considered a single nuclear spin interacting with the electron spin and lattice systems. Nuclear spin-spin coupling of the form

$$\mathcal{H}_{\mathrm{ss}}=\hbar\sum_{\langle i,j\rangle}\mathbf{I}^i\cdot\mathbf{a}(\mathbf{R}^{i-j})\cdot\mathbf{I}^j \quad (9)$$

causes the transverse relaxation, decay of the magnetization perpendicular to the external field. A trivial source of such coupling is the direct nuclear dipole interaction. In magnetic materials, however, the Rudermann-Kittel-Kasuya-Yosida interaction mediated by electron spin systems is usually more important and is given by[33–35]

$$a_\alpha(\mathbf{R})=\frac{1}{\hbar(g\mu_B)^2}\sum_{\mathbf{q}}\chi_\alpha(\mathbf{q})|A_\alpha(\mathbf{q})|^2\exp(-i\mathbf{q}\cdot\mathbf{R}). \quad (10)$$

The transverse relaxation is most commonly measured by spin-echo decay, i.e., the spin-echo intensity as a function of the time separation τ between $2/\pi$ and π pulses. When $a_x, a_y \ll a_z$, the coupling a_z leads to a Gaussian spin-echo decay,

$$I(2\tau)=I_0\exp\{-(2\tau)/T_{2L}-(2\tau)^2/(2T_{2G}^2)\}, \quad (11a)$$

$$(1/T_{2G})^2=\frac{c}{8}\sum_{i\neq j}|a_z(\mathbf{R}^{i-j})|^2, \quad (11b)$$

if the measurement is done by NMR on one of the quadrupole split lines. Here c is the abundance of the isotope (0.69 for ^{63}Cu) and $1/T_{2L}$ is the decay rate due to the spin-lattice relaxation process, which can be determined from the measurement of $1/T_1$. Measurements of $1/T_{2G}$ provides important information on the static q-dependent susceptibility $\chi(\mathbf{q})$ of spin systems, which is complementary to the information provided by $1/T_1$.

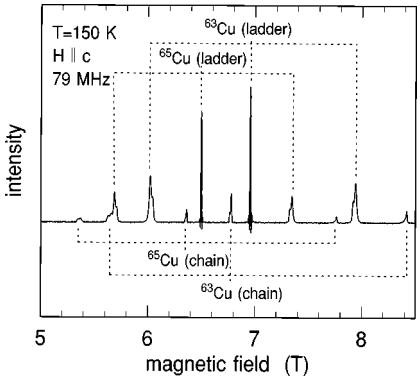

FIG. 3. The spin-echo Cu NMR spectrum at $T=150$ K obtained by sweeping the magnetic field along the c direction at the resonance frequency of 79 MHz.

III. RESULTS AND ANALYSIS

A typical NMR spectrum in $Sr_{14}Cu_{24}O_{41}$ is shown in Fig. 3 obtained at $T=150$ K with a wide sweep range of the magnetic field along the c direction. We observed two sets of lines, corresponding to two distinct sites. Each set consists of six lines, corresponding to three quadrupole split lines (a sharp center line and two broad satellite lines) for both ^{63}Cu and ^{65}Cu isotopes. The assignment of these lines to the chain and the ladder Cu sites are also shown in the figure. The assignment was made first based on the values of the quadrupole splitting ν_α. For one set of lines, we obtained $|\nu_a|=2.6$, $|\nu_b|=13.5$, and $|\nu_c|=10.9$ MHz for ^{63}Cu, which are similar to the values in the two-leg spin-ladder compound $SrCu_2O_3$ (Ref. 36) ($|\nu_b|=10.15$ and $|\nu_a|,|\nu_b|=1.46, 8.69$ MHz) and hence assigned to the ladder Cu sites. The other set assigned to the chain Cu sites shows approximate axial symmetry of EFG around the b axis with $|\nu_b|=32$ MHz. Such symmetry is expected only for the chain sites. Indeed a similar result has been obtained for the spin-Peierls compound $CuGeO_3$ that has similar chain structure as $|\nu_\alpha|=(19.7,34.0,14.3)$ MHz.[37] These assignments are more firmly supported by their distinct temperature dependences of K and $1/T_1$, as will be discussed in detail below. Our site assignment is consistent with other groups[21,22] based on the NQR and powder NMR spectra.

The spectrum in Fig. 3 was taken with insufficient spectral resolution due to small gate width set by the boxcar to integrate the spin-echo signal. This results in the spurious wiggle for the narrow center lines at the ladder Cu sites. With improved resolution, the individual resonance lines in Fig. 3 show rich fine structure, as will be shown in later sections.

We found a third set of NMR lines at low temperatures. An example of the ^{63}Cu center line is shown in Fig. 4. The main line at 8.37 T comes from the ladder sites. A new line appears near 8.33 T below 30 K. As we discuss in detail in Sec. III B 1, we conclude that this line comes from those chain sites which carry spin-1/2 and participate in dimer formation. Other chain lines shown in Fig. 3, which can be observed at higher temperatures, belong to the Zhang-Rice (ZR) singlet sites, whose d spin forms a bound singlet with a hole spin on the neighboring oxygen sites. In the following, we present the results of NMR/NQR spectra, magnetic shift, EFG, $1/T_1$, and $1/T_{2G}$ for the ladder and the chain sites separately.

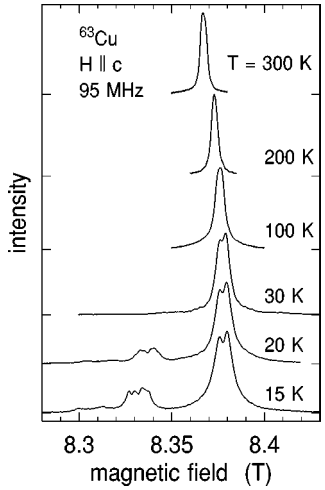

FIG. 4. Temperature variation of the ^{63}Cu center line NMR spectrum with the magnetic field along the c direction at 95 MHz. A new line appears below 30 K.

A. Ladder Cu sites

1. NMR/NQR spectra, magnetic shift, and EFG

Although the center line of the ladder sites shows a sharp single peak as shown in Fig. 4 except for weak splitting at low temperatures, the satellite lines are broader and show temperature-dependent line shape with several peaks as shown in Fig. 5. This indicates a distribution of ν_α among the ladder sites. This is not surprising since the incommensurate lattice mismatch between chains and ladders can cause local lattice distortion in both subunits with long spatial period. Also distribution of localized holes can produce modulation of ν_α. Following the procedure described in Sec. II, the values of the magnetic shift K_α and ν_α were determined at each peak of the satellite spectrum for three directions of the magnetic field and are shown in Figs. 6 and 7. The values of K_α for different peaks are nearly identical except for K_b

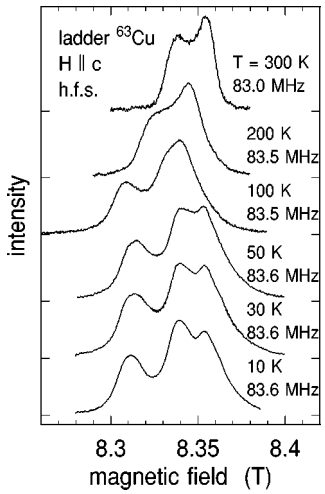

FIG. 5. Temperature variation of the high-field satellite NMR spectrum at the ladder ^{63}Cu sites with the magnetic field along the c direction.

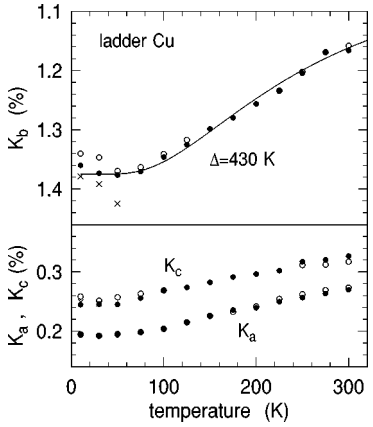

FIG. 6. Temperature dependence of the shift at the ladder Cu sites, determined from the satellite NMR spectra. The different symbols correspond to different peaks in the spectra. The line is the fit to the theoretical expression of $\chi_{\rm spin}$ for an undoped spin ladder.

below 50 K, indicating that ladder sites are magnetically rather homogeneous. The overall temperature dependence of K_b is consistent with the theoretical result for the spin susceptibility of an undoped spin ladder[38] $\chi_{\rm spin}\propto\exp(-\Delta/T)/\sqrt{T}$ with $\Delta=430$ K as shown by the solid line. Although this formula is valid in the low-temperature limit ($T\ll\Delta$), it is indistinguishable from more accurate results[39] in the temperature range studied. The value of Δ is nearly identical to that in $SrCu_2O_3$ (420 K).[9]

If we assume that $\chi_{\rm spin}=0$ at $T=0$, the values of K_α in the low-temperature limit give the orbital shift $K_{\rm orb}$ in Eq. (3), which should be independent of temperature. We obtain $K_{a,\rm orb}=0.19$, $K_{b,\rm orb}=1.37$, and $K_{c,\rm orb}=0.25\%$, which are close to the values in $SrCu_2O_3$,[36] $K_{\parallel,\rm orb}=0.29$ and $K_{\perp,\rm orb}=1.31\%$ for the parallel and perpendicular direction to the ladder plane. They are also close to the values in high-T_c cuprates. For example, $K_{\parallel,\rm orb}=0.28$ and $K_{\perp,\rm orb}=1.28\%$ for $YBa_2Cu_3O_7$.[40] This indicates that the $d_{x^2-y^2}$ wave function accommodating Cu spins and the crystal-field splitting of the d levels are common to all these cuprates. There is a large anisotropy also in $K_{\rm spin}$. Since $\chi_{\rm spin}$ is expected to be nearly isotropic except for the anisotropy of the g value,[41] the anisotropy of $K_{\rm spin}$ should be ascribed to the anisotropy of the

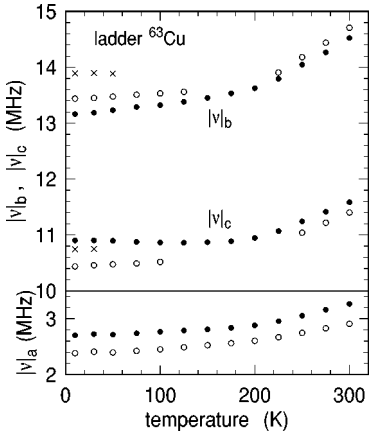

FIG. 7. Temperature dependence of the quadrupole splitting at the ladder ^{63}Cu sites. The different symbols correspond to different peaks in the satellite NMR spectra.

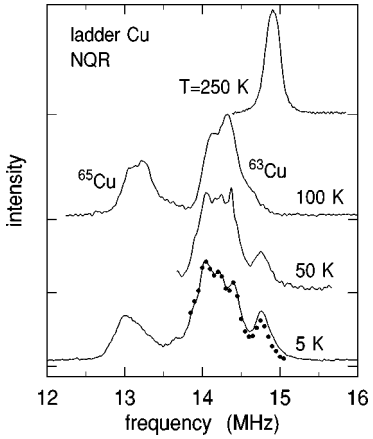

FIG. 8. Temperature variation of the NQR spectrum at the ladder Cu sites. The lines are obtained by adding the Fourier-transformed spectra of the spin-echo signal as described in the text, which agree with the result of point by point measurements shown by the dots.

hyperfine coupling constant $A_\alpha(\mathbf{q}=0)$. It is negative and large for the b direction and positive and small for other directions. By plotting K_c and K_a against K_b, the anisotropy of $A_\alpha(0)$ was obtained as

$$A_a(0):A_b(0):A_c(0)=0.35\pm0.02:-1:0.35\pm0.03. \tag{12}$$

The quadrupole coupling constant $|\nu_\alpha|$ shows an interesting temperature dependence (Fig. 7). It depends on temperature only weakly below 200 K, however, increases steeply above 200 K. The NQR spectrum also changes with temperature as shown in Fig. 8. At 5 K, the ^{63}Cu spectrum shows a main line with three peaks in the frequency range 14–14.4 MHz and another distinct peak at 14.7 MHz. As the temperature is raised the high-frequency peak becomes weaker and merges into the main line. The three peak structure of the main line also becomes obscure. Above 100 K, the entire spectrum becomes narrower and moves to higher frequency, which is consistent with the increase of $|\nu_\alpha|$ for all α. Although the NQR spectrum at 250 K shows a sharp single peak, this must be a coincidence since the satellite spectra for high-field NMR show multipeak structure at all temperatures (see Fig. 5).

2. NQR nuclear spin-lattice relaxation rate

We first attempted to measure $1/T_1$ using high-field NMR at about 8 T assuming that the relaxation process is magnetic. However, the recovery curve did not fit the theoretical expression Eq. (7). This has not been noted in the previous experiments.[21–23] Comparison of the recovery curves for ^{63}Cu and ^{65}Cu then showed that the relaxation process is dominantly quadrupolar in a wide temperature range. This is an unusual situation for a spin system, for which one would naturally expect that coupling to electron spins is the major source for nuclear relaxation. Since the recovery curve for quadrupole relaxation in high-field NMR cannot be determined uniquely, we measured $1/T_1$ using zero-field NQR. We found that a single exponential function Eq. (5) fits the

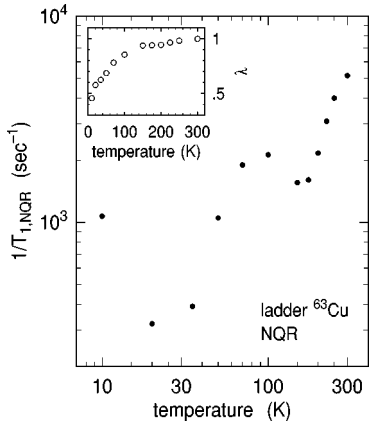

FIG. 9. Temperature dependence of $1/T_{1,\mathrm{NQR}}$ at the ladder ^{63}Cu sites obtained by fitting the recovery curve to the stretched exponential form Eq. (13). In the inset is shown the temperature dependence of the stretch exponent λ.

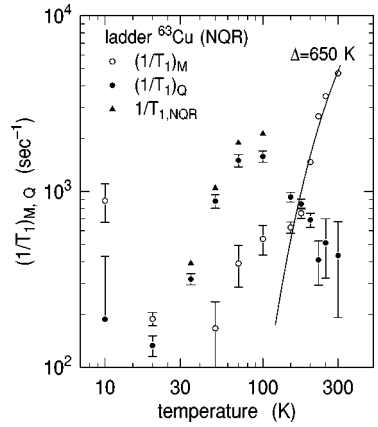

FIG. 11. Temperature dependences of the magnetic $(1/T_1)_M$ and quadrupole $(1/T_1)_Q$ contributions to $1/T_{1,\mathrm{NMR}}$ are separately shown. The line represents an activated temperature dependence with $\Delta = 650$ K.

NQR recovery curve above 200 K but it fails at lower temperatures, indicating a distribution of $1/T_1$. We then used a stretched-exponential form

$$I(t) = I_\infty - \{I_\infty - I(0)\}\exp\{-(t/T_{1,\mathrm{NQR}})^\lambda\}, \qquad (13)$$

to parametrize the distribution, which fits the data well at all temperatures over more than two decades.

Measurements were done at the center of the main NQR line and the values of $1/T_{1,\mathrm{NQR}}$ and λ for ^{63}Cu are plotted in Fig. 9. Above $T = 200$ K, $1/T_1$ increases strongly with increasing temperature. But it shows a minimum around 150 K and a broad maximum near 100 K. The distribution of $1/T_1$ (deviation of λ from 1) also starts to develop in this temperature range as shown in the inset. The isotopic ratio of $1/T_{1,\mathrm{NQR}}$ is plotted in Fig. 10. The relaxation is almost entirely magnetic above 200 K but quadrupole contribution appears below 200 K and becomes dominant below 100 K. This ratio turns to magnetic again below 20 K. This is presumably due to magnetic impurities, which cause an upturn of $1/T_1$ at very low temperatures. Following the method explained in Sec. II, the magnetic and the quadrupole contributions for ^{63}Cu are separated and plotted in Fig. 11.

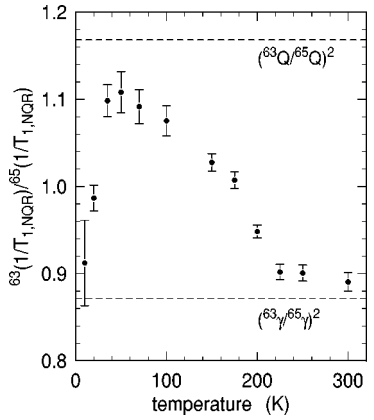

FIG. 10. Temperature dependence of the ratio of $1/T_{1,\mathrm{NQR}}$ for the two Cu isotopes at the ladder sites. The dashed lines indicate the expected ratio if the nuclear relaxation is entirely magnetic or quadrupolar.

The magnetic contribution $(1/T_1)_M$ shows approximately an activated temperature dependence above 150 K, with the activation energy $\Delta = 650$ K, which is between the two previous results on powder samples, 735 K by Akimitsu *et al.*[21] and 470 K by Tsuji *et al.*[22,23] Our value of Δ is very close to that observed in the two-leg spin-ladder material $SrCu_2O_3$ (680 K) by Ishida *et al.*[36] but considerably larger than the activation energy for χ_{spin} (430 ± 50 K, Fig. 6). Such a discrepancy has been noted also in $SrCu_2O_3$ (Ref. 9) and other quantum spin chains with a spin gap.[42,43] Recently theories[44,45] have been proposed to explain it.

The quadrupole contribution $(1/T_1)_Q$ shows a pronounced peak near 100 K. Such a peak is explained most naturally by the classical theory of motional effects.[46] In analogy to Eq. (8) for magnetic processes, $(1/T_1)_Q$ is given by the spectral density of EFG fluctuations at the NQR frequency ω_0. The width of this spectral density is generally given by $1/\tau_c$, the inverse correlation time of EFG fluctuations. If the instantaneous amplitude of EFG fluctuations, i.e., the integral of the spectral density over frequency, is constant, $(1/T_1)_Q$ becomes largest when $1/\tau_c = \omega_0$. Since $1/\tau_c$ should increase with temperature, a peak of $(1/T_1)_Q$ is expected when this condition is met. To quantify this picture, we assume an exponential correlation function $\exp(-t/\tau_c)$. Then

$$\left(\frac{1}{T_1}\right)_Q = K\frac{2\tau_c}{1+(\omega_0\tau_c)^2}. \qquad (14)$$

The constant K is determined by the maximum value of $(1/T_1)_Q$ ($=1700\ \mathrm{s}^{-1}$) since $\omega_0\tau_c = 1$ at the maximum. Then $1/\tau_c$ can be calculated as a function of temperature from the data of $(1/T_1)_Q$ and is plotted against $1/T$ in Fig. 12. It shows approximately an activated temperature dependence with $\Delta = 230$ K. A likely source of the EFG fluctuations is the motion of holes in the ladders. However, the value of Δ is an order of magnitude smaller than the activation energy for the electrical conductivity (2200 K).[18] There is *a priori* no reason to assume that the amplitude of the EFG fluctuations (K) is independent of temperature. However, since the amplitude most likely increases monotonically with temperature, the peak in $(1/T_1)_Q$ must be caused primarily by the temperature variation of $1/\tau_c$.

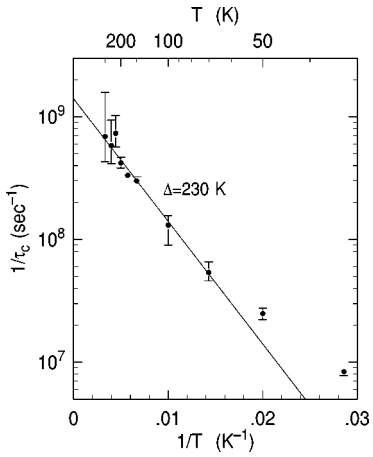

FIG. 12. Temperature dependences of the inverse correlation time of the EFG fluctuations. The line represents an activated temperature dependence with $\Delta = 230$ K.

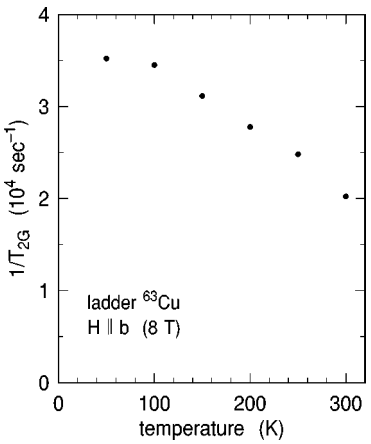

FIG. 14. Temperature dependence of the Gaussian spin-echo decay rate at the ladder ^{63}Cu sites measured on the NMR center line with the magnetic field of 8 T along the b direction.

If this model is correct, $(1/T_1)_Q$ should show a $1/\omega_0^2$ frequency dependence at low temperatures where $\omega_0 \tau_c \gg 1$. Since frequency is fixed in NQR experiments, we have to use high field NMR to check this. We note that even though the functional form of the NMR recovery curve is not known for a quadrupolar process, it must be a unique function of t/T_1. Thus two recovery curves with different $1/T_1$ should coincide by an appropriate change of the time scale. This is demonstrated in Fig. 13. We measured the recovery curve for the ^{63}Cu center line at three frequencies at $T = 50$ K, where the isotopic ratio of $1/T_1$ becomes largest. The recovery curves are plotted against κt, where κ is 1 at 95 MHz and, at other frequencies, chosen so that all curves lie on top of each other. The frequency dependence of κ is plotted in the inset in a log-log scale, which leads to the relation $(1/T_1)_Q \propto \omega^{-1.14}$. This frequency dependence is weaker than the ω^{-2} dependence predicted by Eq. (14). It should be noted, however, that the magnetic contribution is not completely negligible and distribution of τ_c can also lead to a weaker ω dependence.

Since the NQR frequency, which is proportional to Q, is different for two isotopes and $(1/T_1)_Q$ depends on frequency

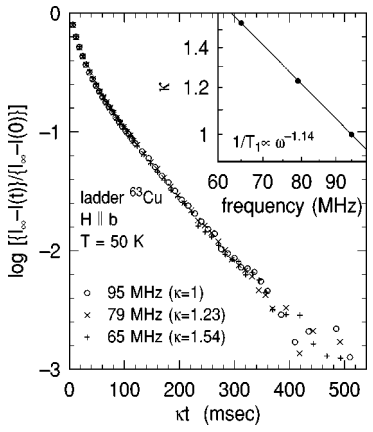

FIG. 13. The inversion recovery curves at $T = 50$ K for ^{63}Cu NMR center line taken at three different frequencies are shown to coincide by proper rescaling of the time axis. The inset shows the frequency dependence of $1/T_1$ in a log-log scale.

at low temperatures, the method of separating magnetic and quadrupolar contribution described below Eq. (6) is strictly not correct. In fact, the relaxation could be entirely quadrupolar below 100 K, in which case $(1/T_1)_Q$ is simply given by the measured $1/T_{1,NQR}$ shown by the triangles in Fig. 11. The difference, however, is not significant and should not change the qualitative feature of the analysis presented above.

3. Spin-echo decay

The spin-echo decay was measured for the center line of the ladder ^{63}Cu sites in a magnetic field of 8 T along the b direction. The data can be fit to Eq. (11a) with T_{2L} and T_{2G} as fitting parameters. The temperature dependence of $1/T_{2G}$ is shown in Fig. 14. At all temperatures $1/T_{2L}$ is more than an order of magnitude smaller than $1/T_{2G}$. The exchange interaction in spin ladders is expected to give rise to short-range antiferromagnetic correlations and, therefore, a peak of $\chi(\mathbf{q})$ at $\mathbf{q} = (\pi, \pi)$. As temperature is decreased, $1/T_{2G}$ increases gradually and saturates at a finite value below about 100 K. This indicates the growth of $\chi(\pi, \pi)$ and the antiferromgnatic correlation length and subsequent saturation, consistent with a spin gap of about 400 K. Similar behavior has been observed in the two-leg spin-ladder compound $SrCu_2O_3$,[47] and in qualitative agreement with the Monte Carlo calculation by Sandvik *et al.*[48]

B. Chain Cu sites

1. NMR/NQR spectra and magnetic shift

We show in Fig. 15 the ^{63}Cu center line spectra at the chain sites in the magnetic field along the b direction. At low temperatures below 50 K, the spectra show many sharp peaks, indicating that there are many inequivalent chain Cu sites with different values of magnetic shift and/or EFG. This is again what one would expect, since either the lattice mismatch between chains and ladders or distribution of localized holes can make many inequivalent chain Cu sites. However, the spectra can be naturally divided into two groups of lines, A and B as indicated in the figure, each of which moves rather rigidly as temperature is changed below 50 K. This indicates that the temperature variation of the shift is similar

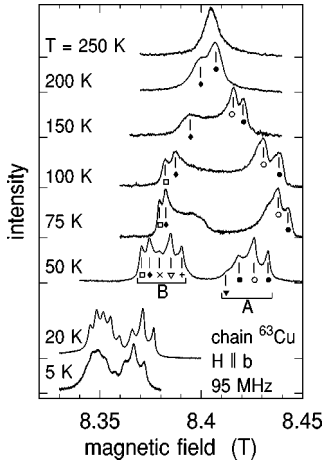

FIG. 15. Temperature variation of the center line NMR spectrum at the chain ^{63}Cu sites obtained at 95 MHz for $H\|b$.

within each group but quite different between them. The spectra for the two sites are well separated below 50 K with the intensity ratio $I_A/I_B=0.65\pm0.1$. Above 50 K, substantial changes occur in the line shape. Each peak gets broadened and sharp structure becomes obscure. At the same time, the region between A and B lines is being gradually filled up, until finally the whole spectrum collapses into a broad single line above 250 K.

The magnetic shift at each peak was determined from the center line spectra at 95 and 75 MHz and are shown in Fig. 16. The different symbols correspond to those shown in the spectra in Fig. 15 and indicate at which peak the shift was measured. The two groups show quite contrasting behaviors. The temperature dependence of K_b at A sites is similar to the susceptibility data below 200 K. The solid line in Fig. 16 is the calculation for a dimer model, $\chi_{Db}=N_A(g_b\mu_B)^2/k_BT[3+\exp(J/k_BT)]$ with $J=130$ K, which explains well the bulk susceptibility below 200 K (Fig. 2).[49] The shift at the B sites show a similar temperature dependence at low temperatures

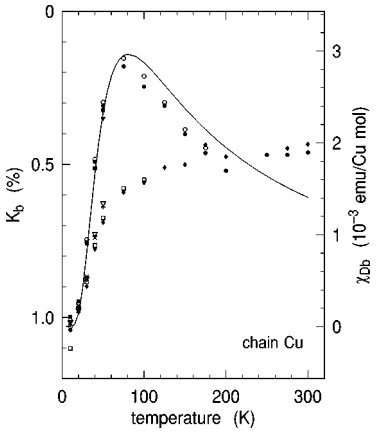

FIG. 16. Temperature dependence of the shift along the b direction at the chain ^{63}Cu sites obtained from the spectra in Fig. 15 and similar spectra at 79 MHz. The symbols correspond to those shown in Fig. 15 and indicate at which peak the shift was measured. The line is the calculated susceptibility for the dimer model (per mole of dimer Cu sites) with $J=130$ K. The proportionality constant between the scales for K_b and χ gives the hyperfine coupling constants $A_b(0)/(2\hbar\gamma_n)=-1.89$ T.

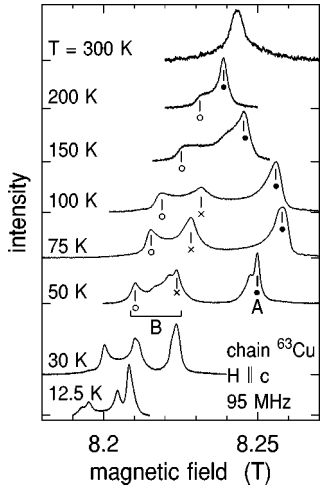

FIG. 17. Temperature variation of the center line NMR spectrum at the chain ^{63}Cu sites obtained at 95 MHz for $H\|c$.

(below 50 K) but the temperature variation $|dK_b/dT|$ is about half as large as that for the A sites. However, instead of having a peak, K_b at the B sites keeps decreasing above 50 K, where the drastic change of the line shape occurs. Above 250 K, where the entire spectrum collapses into a single symmetric line, K_b decreases slightly in contrast to the decrease of χ.

Similar features are observed for other field directions. The spectra and the shift for $H\|c$ are shown in Figs. 17 and 18. Again the spectra consist of two groups of lines at low temperatures, although the peak structure within each group is less clear than that for $H\|b$. Below 50 K, the A sites show twice as large a temperature variation of K_c as the B sites. However, above 50 K the spectra for both sites get broadened and begin to merge together, until the whole line collapses into a single peak above 250 K. The shift at the A sites shows a similar temperature dependence as χ but the behavior at the B sites is quite different.

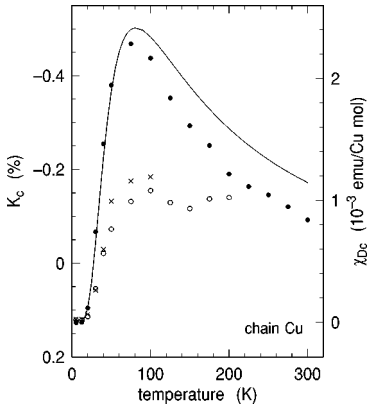

FIG. 18. Temperature dependence of the shift along the c direction at the chain ^{63}Cu sites obtained from the spectra in Fig. 17 and similar spectra at 79 MHz. The symbols correspond to those shown in Fig. 17. The dots show the data for A sites. The circles and the crosses show the data for B sites. The line is the calculated susceptibility for the dimer model (per mole of dimer Cu sites) with $J=130$ K. The proportionality constant between the scales for K_b and χ gives the hyperfine coupling constants $A_c(0)/(2\hbar\gamma_n)=-1.48$ T.

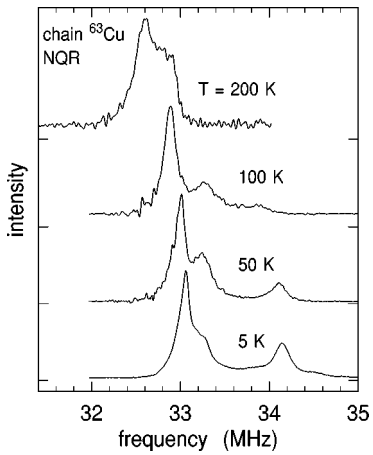

FIG. 19. Temperature variation of the NQR spectrum at the chain ^{63}Cu sites.

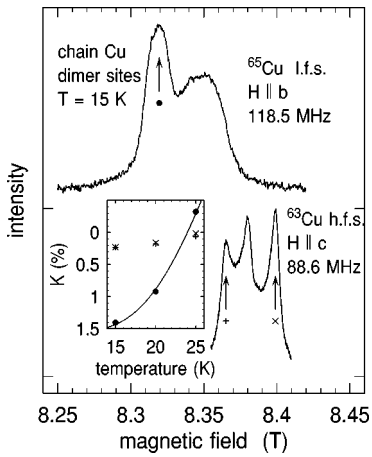

FIG. 20. The NMR satellite spectra at the dimer chain sites at $T=15$ K. The upper spectrum is the low-field satellite for $H\|b$ for ^{65}Cu and the lower spectrum is the high-field satellite for $H\|c$ for ^{63}Cu. The inset shows the temperature dependence of the shift at peaks shown in the spectra. (The dots are for $H\|b$ and crosses and plus marks are for $H\|c$.)

The temperature variation of the NQR spectrum at the chain Cu sites shown in Fig. 19 also reveals the tendency that the clear site distinction observed at low temperatures becomes gradually averaged out with increasing temperature. Comparison of $1/T_1$ measured by NMR and NQR indicates that the strong lowest frequency NQR peak (33.0 MHz at 50 K) corresponds to the A sites and the two higher frequency NQR peaks (33.2 and 34.1 MHz at 50 K) to the B sites.

Since the A sites show a stronger temperature dependence of shift than the B sites at low temperatures, that is to say the A sites are more magnetic than the B sites, it is tempting to assign the A sites to the dimer sites which carry spin-1/2 and the B sites to the ZR singlet sites bound to oxygen holes and ascribe the averaging behavior between A and B sites at high temperatures to the motion of holes. Such interpretation, however, is incompatible with the anisotropy and the magnitude of the hyperfine coupling constant $\mathbf{A}^{i-j}$ as we discuss below.

If we assume that A sites were the dimer sites whose susceptibility is shown by the solid lines in Figs. 16 and 18, the proportionality constant between K and χ gives the value of $\mathbf{A}(\mathbf{q}=0)$ as $A_b(0)/(2\hbar\gamma_n)=-1.89$ and $A_c(0)/(2\hbar\gamma_n)=-1.48$ T. In general, $\mathbf{A}(0)$ includes the anisotropic on-site coupling $\mathbf{A}^0$ and the isotropic nearest-neighbor coupling A^1.[50] If both neighbor sites carry spin-1/2, $\mathbf{A}(0)=\mathbf{A}^0+2A^1$. But if one or both of them are the ZR singlet with no active spin, $\mathbf{A}(0)=\mathbf{A}^0+A^1$ or $\mathbf{A}^0$, respectively. The on-site term $\mathbf{A}^0$ is determined by the $d_{x^2-y^2}$ wave function and common to all cuprates. The nearest-neighbor coupling A^1 is quite large in high-T_c cuprates with 180° Cu-O-Cu bond angle ($A^1/(2\hbar\gamma_n)=4-6$ T) but should be much smaller for the chain Cu sites in $Sr_{14}Cu_{24}O_{41}$ with 90° bond angle. Note that the magnitude of A^1 and superexchange should correlate.

Detailed results of the hyperfine coupling has been obtained in the spin-Peierls compound $CuGeO_3$ by Itoh *et al.*[51] and Fagot-Revurat *et al.*[52] as $A_b(0)/(2\hbar\gamma_n)=-24$, $A_a(0)/(2\hbar\gamma_n)=-3.0$, and $A_c(0)/(2\hbar\gamma_n)=-2.3$ T. The nearest-neighbor coupling $A^1/(2\hbar\gamma_n)$ in $CuGeO_3$ is estimated to be at most about 1.0 T.[52] These results provide a reasonable estimate for the hyperfine coupling constants at the chain Cu sites in $Sr_{14}Cu_{24}O_{41}$, since both materials have similar chain structure. Then, independent of the type of neighboring sites, $\mathbf{A}(0)$ at the dimer sites should be strongly anisotropic, $|A_b(0)|\gg|A_c(0)|,|A_a(0)|$, with negative $A_b(0)$. For the ZR singlet sites, for which the on-site coupling is absent, $\mathbf{A}(0)=nA^1$, where $n=0$, 1, or 2 is the number of nearest neighbors carrying an active spin. Thus $|A_b(0)|_{\rm dimer}\gg|A_b(0)|_{\rm ZR}$.

The hyperfine coupling constants at A and B sites are totally inconsistent with these expectations. The value $|A_b(0)|/(2\hbar\gamma_n)=-1.89$ T is much too small and the anisotropy $|A_c(0)|/|A_b(0)|=0.78$ is too large if the A sites were the dimer sites. Moreover, the difference of $|A_b(0)|$ for A and B sites is only a factor of 2, whereas an order of magnitude difference is expected for the dimer and the ZR singlet sites. Thus we are led to conclude that all the chain NMR signal shown in Figs. 15 and 17 originate from the ZR singlet sites.

It turned out that the signal from the dimer chain sites can be observed only at low temperatures (below 30 K) because T_2 becomes too short at higher temperatures. An example was shown in Fig. 4 where a new set of lines emerges near 8.33 T. Following the procedure outlined in Sec. II, the central and the satellite lines corresponding to this group of lines have been identified. Examples of the satellite spectra are shown in Fig. 20. For $H\|b$ a spectrum for ^{65}Cu nuclei is shown since ^{63}Cu lines for the dimer sites overlap with other lines. The satellite spectra for the dimer sites have several distinct peaks, again indicating the existence of microscopically inequivalent sites. The quadrupole splitting was obtained as $|\nu_b|=17.8$ and $|\nu_c|=6.4$ MHz for ^{63}Cu. From the satellite spectra for $H\|b$, the intensity ratio for the dimer and the ZR sites is obtained as $I_{\rm dimer}/I_{\rm ZR}=0.39\pm0.1$ after correcting for the spin-echo decay, indicating that there are about three dimer sites per formula unit. The shift was obtained for the peaks in the satellite spectra and are shown in the inset of Fig. 20. Although the measurements are limited to a narrow temperature range, the shift shows right behavior expected for the dimer sites. First the data is consistent with the large and negative $A_b(0)$. The solid line in the inset is the fit to the dimer model with $A_b(0)/(2\hbar\gamma_n)=-24$ T, which gives $J=126$ K, in good agreement with the analysis of the

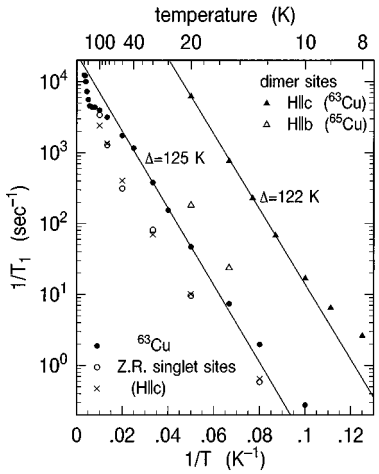

FIG. 21. Temperature dependence of $1/T_1$ at the chain sites. The dots, circles, and crosses show the results for the ^{63}Cu ZR singlet sites measured on the NMR center lines at 95 MHz for $H\|c$. The symbols correspond to those shown in Fig. 17. The dots show the data for A sites. The circles and the crosses show the data for B sites. The solid and open triangles show the results for the dimer sites for $H\|b$ (obtained at the main peak of the ^{65}Cu low-field satellite NMR spectrum at 101 MHz) and for $H\|c$ (obtained at the middle peak of the ^{63}Cu high-field satellite NMR spectrum at 88.6 MHz), respectively.

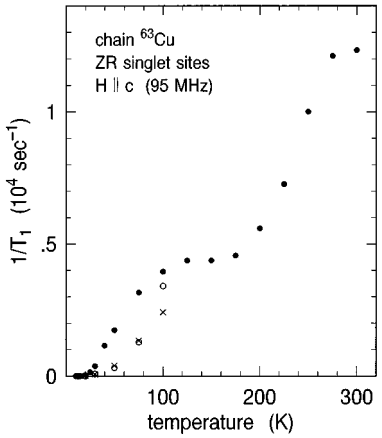

FIG. 22. Temperature dependence of $1/T_1$ at the ZR singlet sites plotted in a linear scale. The data are the same as those shown in Fig. 21.

susceptibility data ($J=130$ K). Second it shows the expected anisotropy. By comparing the temperature variation of K_b and K_c, we obtain $A_c(0)/A_b(0)=0.12$ in good agreement with the result in $CuGeO_3$. A more decisive evidence for the assignment of these lines to the dimer sites comes from the spin-echo decay measurements as we describe later.

2. NMR nuclear spin-lattice relaxation rate

High field NMR was used to measure $1/T_1$ at both the ZR singlet and the dimer chain Cu sites. The results are plotted against $1/T$ in Fig. 21. Unlike the ladder sites, the relaxation was confirmed to be entirely magnetic in the whole temperature range and recovery curves were fit well by Eq. (7). We first discuss the results for the ZR singlet sites for $H\|c$ measured on the center lines, which are shown by dots, circles, and crosses. The different symbols correspond to those shown in Fig. 17 and indicate at which peak the measurements were done. A clear activated temperature dependence with a gap of 125 K is observed below 50 K over nearly four decades of $1/T_1$, which is in fair agreement with the previous powder NQR results.[22,23] The A and B sites show a factor of about 4 difference in the magnitude of $1/T_1$. This is consistent with the factor of 2 difference in the hyperfine coupling constant mentioned in the previous subsection. At low temperatures, T_1 becomes quite long ($\sim$10 s) and still keeps increasing. This is in contrast to the results for the ladder sites, which show fast relaxation at low temperatures due to magnetic impurities. Above 50 K, the difference of $1/T_1$ between the A and B sites becomes smaller, which is consistent with the change in the spectrum (Figs. 15 and 17) showing the gradual averaging between the two sites. An anomalous behavior is observed at high temperatures as shown in Fig. 22. There is a plateau between 100 and 200 K, above which $1/T_1$ increases steeply again. Note that there is also an anomaly in K_b (Fig. 16) above 200 K.

Let us turn to the results on the dimer sites shown by the solid and open triangles in Fig. 21 obtained for the satellite lines. A nearly identical activation energy (122 K) is obtained for the dimer sites, indicating that the same spin fluctuations cause the relaxation at both the dimer and the ZR singlet sites. There is a large anisotropy $(1/T_1)_c/(1/T_1)_b \simeq 30$, which is consistent with the anisotropy in the hyperfine coupling constant $A_c(0)/A_b(0)=0.12$. We observed a strong frequency dependence of $1/T_1$ at the dimer sites. The data in Fig. 21 for $H\|c$ are obtained at 88.6 MHz. At $T=20$ K, the value of $1/T_1$ measured at 101 MHz is smaller by a factor 1.72. If a power-law frequency dependence is assumed, this means $1/T_1 \propto \omega^{1.8}$. We have confirmed that $1/T_1$ depends on frequency not on magnetic field by comparing the values of $1/T_1$ measured on the two satellite lines. They are equal when measured at the same frequency with different magnetic fields. Further detailed study over wider temperature and frequency ranges is clearly necessary.

3. Spin-echo oscillation

The most striking result on the dimer chain sites is the giant oscillation of spin-echo intensity as shown in Fig. 23. In the main panel, we plot the spin-echo intensity of the ^{63}Cu center line against 2τ, where τ is the separation between the $\pi/2$ and π rf pulses, obtained at $H=8.9217$ T along the b direction, $f=95$ MHz and $T=10$ K. Instead of a monotonic Gaussian or exponential decay, it shows a clear oscillation with a beat. A third beat was observed near $2\tau=1.2$ ms (not shown in the figure), indicating that the beat is also periodic. A similar oscillation was also observed for ^{65}Cu. The isotopic ratio of the period of the oscillation and the beat is equal to $(^{65}\gamma_n/^{63}\gamma_n)^2=1.15$, indicating that the oscillation is due to nuclear spin-spin coupling.

There are a few conditions to observe such a clear oscillation. First, the center line spectra of the ladder sites and the dimer sites overlap at this temperature and field direction. To minimize the contribution from the ladder sites and achieve good spectral resolution, the echo-decay data was taken by integrating the digitized echo signal over a long enough time

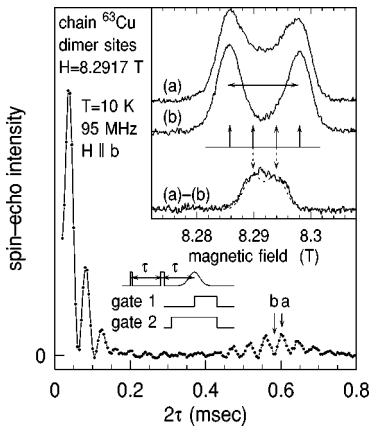

FIG. 23. Main panel: The spin-echo intensity of the ^{63}Cu center line at the dimer chain sites is plotted against 2τ. The data were obtained by integrating one side of the digitized echo signal (gate 1) at $T=10$ K and $f=95$ MHz with the magnetic field of 8.2917 T along the b direction. Inset: The upper two spectra were obtained by integrating both side of the spin-echo signal by a box-car averager (gate 2) at the top (point a, $2\tau=0.6026$ msec) and the bottom (point b, $2\tau=0.5826$ mse) of the oscillation. The lowest spectra is the difference between the upper two spectra and is fit to the sum of two Gaussians shown by the dotted line. Also illustrated in the inset is the splitting of the NMR center line spectra due to the spin-spin coupling as described in the text.

interval on one side of the echo peak (gate 1 in the illustration of Fig. 23). It is not possible to integrate the echo signal on both side of the peak (gate 2) for short τ. We found that the clear oscillation was observed only at a specific value of the magnetic field. Since the ladder sites show a fast Gaussian spin-echo decay ($T_{2G}=30$ μs, see Fig. 14), the signal at the second beat near $2\tau\sim0.6$ ms comes entirely from the dimer sites. Quite remarkably, the shape of the NMR spectrum depends on the value of τ as shown in the inset of Fig. 23. The upper two spectra were obtained at the top ($2\tau=0.6026$ ms, point a) and the bottom ($2\tau=0.5826$ ms, point b) of the oscillation, respectively, by integrating the spin-echo signal by a boxcar with a wide gate covering both sides of the echo signal (gate 2). The outer region of the spectra is nearly identical but the inner part is largely suppressed for the spectrum at b. This means that the oscillation occurs only in the inner part of the spectrum. The lowest spectrum is the difference between these two spectra. The peak of this spectrum then gives the optimum value of the field to observe the oscillation.

Such a long-lived coherent oscillation implies that nuclear spins are strongly coupled in pairs and the coupling between pairs is very weak. This can be demonstrated naturally from a slightly modified model of Eq. (9),

$$\mathcal{H}_{\rm ss}=\hbar\sum_{\langle i,j\rangle}a_{zz}(\mathbf{R}^{i-j})I_z^iI_z^j, \tag{15}$$

where we have dropped the x and y components of the spin-spin coupling. This is indeed appropriate for the dimer sites for $H\|b$, since $|A_b(\mathbf{q})|\ll|A_a(\mathbf{q})|,|A_c(\mathbf{q})|$. If T_1 is much longer than the time range of the spin-echo decay measurement, I_z can be considered to be static. This also applies to our case since T_1 at $T=10$ K is of the order of 1 s for $H\|b$, while the spin-echo decay was measured over a time range of about 1 ms. In such a case, the evolution of the spin-echo intensity can be calculated exactly. We show the result for $I=1/2$ for simplicity,

$$I(2\tau)=I_0\left\langle\prod_{\langle ij\rangle}\cos(a_{zz}(\mathbf{R}^{ij})\tau)\right\rangle, \tag{16}$$

where the product is taken over the sites occupied by a like spin (same isotope) and $\langle\ \rangle$ indicates the configurational average over the random distribution of different isotopes.

When a nuclear spin is coupled to a large number of other spins, the product of many oscillations with different frequencies and averages over random isotopic configuration quickly destroy the coherent precession. Then Eq. (16) is approximated adequately by a Gaussian in Eq. (11). However, if the nuclear spins are coupled only in pairs, there is a unique frequency, giving rise to a long-lived oscillation. In fact similar oscillations have been observed in many molecules, in which the spin-spin coupling is caused by chemical bonding.[53] Thus the nuclear spin-spin coupling within a dimer is given by the period of the oscillation as $|a_1|/(2\pi)=45$ kHz. The beat shown by the data in Fig. 23 can be explained most naturally by weak coupling between dimers,[54] which provides a second oscillation in the product in Eq. (16). The interdimer coupling is then given by the period of the beat as $|a_2|/(2\pi)=3.4$ kHz, which is an order of magnitude smaller than the intradimer coupling. Thus the spin-echo oscillation data provides direct evidence for well-isolated dimers.

Furthermore, we can estimate the intradimer exchange from the spin-echo oscillation data using Eq. (10). Since A^1 is negligibly small at the dimer sites compared with A_b^0, $A_b(\mathbf{q})$ can be replaced by A_b^0. Then $\hbar a=|A_b^0|^2\chi(\mathbf{R}^{12})|/(g\mu_B)^2$, where $\chi(\mathbf{R}^{12})$ is the nonlocal susceptibility within a dimer describing the response of the second spin when a magnetic field is applied on the first spin. For an isolated dimer, $\chi(\mathbf{R}^{12})/(g\mu_B)^2=-1/(2J)$, therefore, $\hbar a=|A_b^0|^2/(2J)$, where J is the intradimer exchange. Using the observed value of $|a/(2\pi)|=45$ kHz and taking $A_b^0/(2\gamma_n\hbar)=-24$ T from the results for $CuGeO_3$, we obtain $J=156$ K. The agreement between this value and the activation energy of $1/T_1$ (120 K), the gap observed by the neutron-scattering experiment (11 meV),[24] and the value of J obtained from the analysis of χ (130 K) is quite satisfactory, if we consider the uncertainty in value of A_b^0.

Let us now consider the effect of the dimer spin-spin coupling $\mathcal{H}_{\rm dim}=\hbar aI_z^{(1)}I_z^{(2)}$ on the NMR spin-echo spectrum in the static approximation. Suppose we are observing the center line resonance ($I_z=1/2\leftrightarrow-1/2$) of a ^{63}Cu spin $I^{(1)}$. Since there are four possible values of $I_z^{(2)}$ of the second spin ($\pm3/2$, $\pm1/2$), the dimer coupling splits the spectrum into equally spaced four lines. The second spin can be either ^{63}Cu or ^{65}Cu. For the latter case, the coupling a should be larger by a factor $^{65}\gamma_n/^{63}\gamma_n=1.071$, therefore, the spectrum actually consists of eight lines. In spin-echo experiments, one must treat like spin coupling and unlike spin coupling differently. In our case, like spin coupling occurs when $I^{(2)}$ is also a ^{63}Cu spin and $I_z^{(2)}=\pm1/2$. All other cases lead to unlike spin coupling. Thus only two resonance lines out of eight

lines arise from like spin coupling. In the static approximation, unlike spin coupling has no effect on spin-echo decay, therefore, resonance lines associated with unlike spin coupling show spectra which is independent of τ. On the other hand, like spin coupling causes the oscillation of spin-echo amplitude as we have shown above. Thus the spin-echo signal associated with like spin coupling changes sign as a function of τ, i.e. it should be positive when obtained at the top of the oscillation (point a) and negative at the bottom of the oscillation (point b).

This is exactly what we observed as shown in the inset of Fig. 23. The solid arrows indicate the four split lines due to the coupling to a ^{63}Cu spin. Since the outermost two lines are associated with unlike spin coupling ($I_z^{(2)}=\pm 3/2$), they should always give a positive signal. The inner two lines arise from like spin coupling ($I_z^{(2)}=\pm 1/2$), therefore, the spin-echo amplitude should oscillate, positive at point a (solid arrows) and negative at point b (dotted arrows). The two spectra taken at a and b are consistent with these predictions. The spacing between the two peaks in the spectrum at b agrees well with the interval between the outermost two lines indicated by the horizontal arrow.[55] The suppression of the inner region of the spectrum at b can be explained by the sign reversal of the inner two lines. Note that the spectra also include positive contribution from those ^{63}Cu coupled to a ^{65}Cu spin, which should be identical at a and b. The difference between the two spectra shown at the bottom then represents the contribution only from those ^{63}Cu which are coupled to another ^{63}Cu spin in $I_z=\pm 1/2$ states. Ideally, we would expect a double peak separated by a/γ_n, but this could be smeared out by inhomogeneous broadening of the individual lines. Indeed, the spectrum can be fit with a sum of two Gaussians with identical shape displaced by 4.2 mT as shown by the dotted line. This value is in very good agreement with $a/\gamma_n=4.0$ mT determined from the period of the spin-echo oscillation.

IV. DISCUSSION

Although $Sr_{14}Cu_{24}O_{41}$ shows an insulating behavior, many of our results cannot be explained by models including only spin degrees of freedom and suggest that the roles of doped holes and/or lattice dynamics must be considered explicitly. An obvious example is the clear distinction between the dimer and the ZR singlet sites in the chains. The EFG fluctuations at the ladder Cu sites are also likely to be caused by motion of holes. The variation of the NMR/NQR spectra with temperature, which is particularly remarkable at the ZR singlet chain sites, is hard to understand in pure spin models.

A. Ground-state properties and static aspects

We first discuss the ground-state properties and static aspects such as the hole concentration in the chains and ladders, possible charge order, and origin of the dimerization in the chains. The χ data in Fig. 2 suggests that there are four dimer sites per formula unit containing ten chain sites. This is expected if all six holes in the stoichiometric material go into the chain sites. The NMR intensity ratio for the dimer and the ZR sites mentioned in Sec. III B 1 indicates 2.8 ± 0.5 dimer sites per formula unit, although we cannot rule out the possibility that a part of the dimer sites does not contribute to the NMR signal. For the ladder sites, Osafune *et al.* used the optical reflectivity data[27] to estimate the density as one hole per formula unit. A small but finite amount of holes in the ladders is also consistent with the activated temperature dependence of the EFG fluctuation rate $1/\tau_c$, since this is likely to be associated with motion of holes in the ladders. The total number of holes exceeding 6 per formula unit suggests that there are slight excess oxygen and/or Sr deficiencies. Hiroi *et al.*[56] have examined the dependence of χ on the oxygen content. The low-temperature Curie term shows a sharp minimum at the stoichiometric composition. We note, however, that the Curie term of the χ data in Fig. 2, which was obtained for a crystal made in the same conditions as our samples, is as small as this minimum value and corresponds to 0.2 spin-1/2 impurities per formula unit.

It is likely that the doped holes in the chains are arranged in a well ordered manner in space, although no direct evidence of charge order has been reported. This is suggested by the sharp structure of the center line NMR spectra below 50 K in Figs. 15 and 17. The large number of distinct peaks indicates the long period of the superstructure. The sharpness of each peak, whose full width at half maximum (FWHM) is typically 2 mT at 95 MHz, indicates a high degree of periodicity, since disorder would broaden the peak and make them unresolvable. In fact, we observed that each peak further split when the magnetic field is rotated from the symmetric direction. Such a large number of inequivalent sites (close to 20 near the *b* direction) are unlikely to be caused only by the charge order but are probably associated also with the lattice distortion induced by the charge order or by the misfit potential due to the incommensurate *c*-axis ratio between chains and ladders, as discussed by Hiroi *et al.*[56] The lattice distortion will modulate the hyperfine coupling, the orbital shift, and EFG, resulting in many distinct peaks. Such lattice distortion still has to be highly periodic to maintain the sharpness of the peaks.

The apparent absence of disorder-induced broadening and magnetic impurities that could enhance $1/T_1$ at low temperatures characterize the chain subunit as a very clean system. This situation is in sharp contrast to the ladder sites. The center line NMR spectra at the ladder sites (Fig. 4) show at most two peaks which are much broader (FWHM is typically 12 mT at 95 MHz) and impurity spins make a significant contribution to $1/T_1$ at low temperatures (Fig. 11).

The charge order in the chains must be closely related to the dimer formation. Important information has been obtained from neutron-scattering experiments by Matsuda *et al.*[24] The minimum of the excitation energy for chain Cu spins occurs at the wave vector $L/4$ and $L/8$, where $L=2\pi/c_{\text{chain}}$, and the maximum of the scattering intensity is observed at $L/4$. They have concluded that the dimers are formed between Cu sites which are separated by at least twice the nearest-neighbor distance. The nearest-neighbor dimer formation has been ruled out since it would lead to the dispersion minimum and intensity maximum at $L/2$, where no scattering was observed.

Matsuda *et al.*[24] considered models of dimerization both with and without the ZR singlet sites. In the later case, singlet formation among a cluster of 4 or 8 Cu spins was considered, within which the sign of the spin-spin correlation

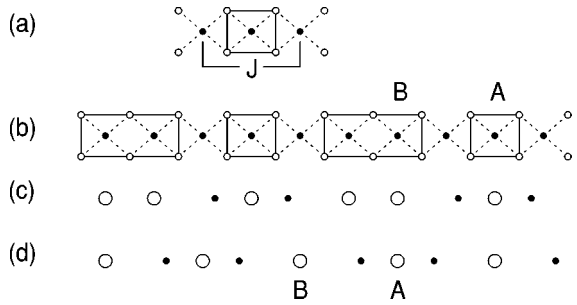

FIG. 24. Schematic illustration of the charge order and dimer formation in the chains. (a) represents the fundamental dimer unit, where two Cu spins separated by a ZR singlet site in the middle are coupled to form a singlet. The solid square shows the four oxygen sites accommodating a hole whose spin is bound to the central Cu spin to form the ZR singlet. (b) Suggested pattern for charge order and dimer formation. The solid rectangle represents the extended ZR singlet consisting of two oxygen holes and two Cu spins. (c) Lattice dimerization that should accompany the spin pairing in (b). Only the Cu sites are shown. The dots and circles represent the dimer and the ZR sites, respectively. (d) An alternative model of spin pairing and lattice dimerization.

function changes as $\langle ++--\rangle$ or $\langle +++++----\rangle$. However, the spin-echo oscillation data indicate a pairwise interaction and more than 60% of the chain sites are expected to be the ZR singlet sites, it is most likely that a dimer unit consists of two Cu spins separated by one ZR singlet sites as shown in Fig. 24(a), which can be represented as $\langle +0-\rangle$. The intradimer exchange then must be the second nearest-neighbor coupling modified by the presence of a ZR singlet in between. It is highly desirable to perform a quantum chemical calculation to see if the superexchange for such a unit can be as large as 130 K.

The spin-echo oscillation data also indicate that the interdimer exchange is more than an order of magnitude smaller than the intradimer exchange. A possible scenario to explain this is that the dimers are separated by at least two nonmagnetic sites. Two such consecutive nonmagnetic sites shown in Fig. 24(b) by a rectangle may be considered as an *extended* ZR singlet, where two oxygen holes and the two Cu spins are bound into a singlet.[57] Thus the charge order and the dimerization may be represented as $\langle +0-\rangle 00\langle +0-\rangle 00\ldots$. In fact this model is qualitatively consistent with all above observations. It provides two inequivalent ZR singlet sites A and B as shown in Fig. 24(b). It should be noted that A sites are coupled to two Cu spins, while B sites are coupled to only one spin, providing a natural explanation for the factor 2 difference in the hyperfine coupling constant at A and B sites as mentioned in Sec. III B 1. Their population ratio in this model is $N_A/N_B=0.5$, which is not very far from the observed intensity ratio $I_A/I_B=0.65\pm0.1$ mentioned in Sec. III B 1. The singlet spin pairing should be accompanied by the lattice dimerization as indicated in Fig. 24(c). If the lattice displacement is large enough, a simpler model of alternating dimer and ZR singlet sites shown in Fig. 24(d) will be also qualitatively consistent with the NMR results. Namely, there are two types of the ZR sites, one within a dimer unit (A) and the other between two dimer units (B). Obviously, the hyperfine coupling should be larger for the A sites. The population ratios in this model $N_A/N_B=N_{\rm dimer}/N_{\rm ZR}=1$, however, is in quantitative disagreement with the observed intensity ratio $I_A/I_B=0.65\pm0.1$ and $I_{\rm dimer}/I_{\rm ZR}=0.39\pm0.1$.

B. High-temperature behavior and dynamic aspects

Let us now turn to the high-temperature behavior and the dynamic aspects. We start with the results in the chain sites, in particular, the drastic temperature variation of the NMR spectral shape at the ZR singlet sites shown in Figs. 15 and 17. The clear distinction of the local magnetic field and the EFG at low temperatures (we will use the term ''local field'' to combine both of them) for many inequivalent sites is gradually being averaged as the temperature increases. Generally, motional effects could be responsible for such a spectral change.[29,30] The distinction of the local field among different sites, whether it is due to charge order or lattice distortion, is static at low temperatures. Thermally induced motion at high temperatures may cause the local field to fluctuate. If the local field jumps between different peaks, the sharp multipeak structure will collapse into a single broad line when the jumping rate $(1/\tau_c)$ becomes comparable to the spacing between the peaks. (We measure the local field in frequency units by multiplying by γ_n.) When the fluctuations become much faster, each nucleus sees only the time-averaged local field, resulting in a narrow line (motional narrowing).

At first sight, this appears to be what is happening at the ZR singlet chain sites. However, unlike the quadrupole relaxation at the ladder sites, the spectral change cannot be ascribed to the temperature variation of $1/\tau_c$. In order to cause narrowing of the whole spectrum, the amplitude of the local-field jump (ΔH) has to be comparable to the spacing between A and B lines ($\sim$40 mT). If the local-field distribution is quasistatic below 50 K $(1/\tau_c \ll \gamma_n \Delta H)$ and fluctuating very fast above 250 K $(1/\tau_c \gg \gamma_n \Delta H)$, it must be that $1/\tau_c \simeq \gamma_n \Delta H$ at some temperature. It is known that the fluctuations of the local field also cause the spin-echo decay. The maximum of $1/T_2 \simeq \gamma_n \Delta H \sim 10^6$ s^{-1} occurs when $1/\tau_c \simeq \gamma_n \Delta H$. Such a fast echo decay should have made the signal completely unobservable. This has not been observed. Although we have not performed detailed spin-echo decay measurements for the ZR singlet sites, the spin-echo signal was observed at $2\tau \simeq 20\mu$s without significant loss of intensity below 200 K. (A peak in $1/T_2$ caused by motional effects has been indeed observed in an organic crystal.[58])

Thus the global change of the spectrum, in particular, the filling of the region between A and B lines near $T=100$ K, must be caused by quasistatic disorder rather than purely dynamic motion. Temperature variation of the lattice displacement with some spatial inhomogeneity may cause such a spectral change, since the transferred hyperfine coupling A^1 is very sensitive to the nearest-neighbor distance. The averaging behavior between A and B sites may be partly explained by decrease of lattice displacement with increasing temperature. The simple dimerization model of Fig. 24(d) is particularly appealing in this regard, since the A and B sites become equivalent when the lattice dimerization disappears. Therefore, the temperature-dependent lattice dimerization alone can account for the global change of the NMR spectrum.

We also note that hole distribution in the chains must be static at least below $T=200$ K. Hopping of holes causes switching between the dimer and the ZR singlet sites. Although the signal from the dimer sites are not observed above $T=30$ K, the large and negative value of $A_b(0)$ implies that the difference of the resonance frequency at the dimer and the ZR sites would be a few MHz at $H=8$ T along the b direction above $T=50$ K. Again the jumping of the local field with such a large amplitude should result in extremely short T_2 at the ZR sites and a significant shift of the resonance field of the ZR sites toward that of the dimer sites, neither of which was observed. Motion of holes might occur at higher temperatures. In fact deviation from the proportionality between K_b and χ (Fig. 16) and the rapid increase of $1/T_1$ (Fig. 22) above $T=200$ K suggest some fundamental change in the magnetic character of the ZR singlet chain sites.

The activation energy of $1/T_1$ at both chain sites (Fig. 21) below $T=50$ K agrees well with the dimerization gap obtained from the χ data and the neutron experiments. This indicates that the spin fluctuations among the excited triplet states cause the nuclear relaxation. The very weak interdimer coupling revealed by the spin-echo oscillation data implies that triplet excitations are nearly localized and the spin fluctuations have a very slow time scale. We suppose that such slow dynamics is responsible for the unusually strong frequency dependence of $1/T_1$ observed at the dimer sites (Sec. III B 2).

We now proceed to the results at the ladder sites. Since the spin-lattice relaxation is a purely dynamic phenomenon, the unusually large quadrupole relaxation rate $(1/T_1)_Q$ at the ladder sites (Figs. 11 and 12) provides clear evidence for motional effects. Since no quadrupole relaxation was observed in the chain sites, this must be caused by charge or lattice motion in the ladder subunit. The temperature dependence of $(1/T_1)_Q$ is quite different from what is expected for ordinary phonons. Usually phonons have temperature independent frequencies but the amplitude of the lattice vibrations increases with temperature, resulting in a monotonic power-law increase of $(1/T_1)_Q$ with temperature. The observed peak in $(1/T_1)_Q$, on the other hand, strongly suggests that it is the time scale of the motion (τ_c) which is most temperature dependent. This is further confirmed by the frequency dependence of $1/T_1$ at a temperature lower than the peak (Fig. 13). Thermally activated hopping of holes between localized states in the ladders appears to be a natural explanation. However, it was noted that the activation energy for $1/\tau_c$ (230 K, Fig. 12) is an order of magnitude smaller than the activation energy for the electrical conductivity (2200 K). Moreover, if we assume $1/\tau_c$ to be the rate of hopping of holes over a distance l, which is of the order of a few lattice constant (~ 10 Å), and use a classical formula to calculate the resistivity,

$$\rho=\frac{k_B T\tau_c}{l^2 n e^2}, \tag{17}$$

we obtain $\rho\sim 10^2$ Ω cm at room temperature for $n=1$ holes per formula unit, which is many orders of magnitude larger than the measured resistivity ($10^{-3}\Omega$ cm) along the most conducting c axis. The EFG fluctuations are too slow to account for the conductivity, therefore, they must be caused by different types of motion. The ladder sites also show some temperature variation of the spectrum, in particular, the NQR line shape (Fig. 8). This is presumably due to the same motion which causes the quadrupolar relaxation.

The magnetic relaxation $(1/T_1)_M$ at high temperatures above 200 K shows an activated behavior indicating a spin gap in the ladder subunit. The activation energy (650 K) is close to the value obtained for the undoped ladder material $SrCu_2O_3$ (670 K). However, since the resistivity and $(1/T_1)_Q$ data indicate that holes in the ladders are reasonably well mobile at this temperature range, it is interesting to ask if the spin excitations are still described by the Heisenberg ladder model or substantially modified by the mobile holes. An important point is that in undoped spin ladders, the spectral weight of the low-frequency ($\omega\ll\Delta$) spin fluctuations at low temperatures ($T\ll\Delta$) appears only near $\mathbf{q}\sim 0$, even though the high-frequency spin fluctuations have dominant weight near $\mathbf{q}\sim(\pi,\pi)$, as pointed out by Troyer *et al.*[38] We can understand this from the expression for the spin-correlation function,

$$S_\alpha(\mathbf{q},\omega)=\sum_{n,m}|\langle m|S_\alpha(\mathbf{q})|n\rangle|^2\delta(E_m-E_n-\omega)\times\exp(-\beta E_n)/Z. \tag{18}$$

For small ω, both $|m\rangle$ and $|n\rangle$ have to be excited states with nearly equal energies ($E_n\simeq E_m$). Since $S_\alpha(\mathbf{q})$ has a nonzero matrix element between magnons at $\mathbf{k}$ and $\mathbf{k}+\mathbf{q}$ and magnons are thermally excited only near the bottom of the dispersion at (π,π), both $\mathbf{k}$ and $\mathbf{k}+\mathbf{q}$ have to be close to (π,π), therefore, $\mathbf{q}$ must be small. When holes are doped, they may cause damping of the magnon mode and spin fluctuations near $\mathbf{q}\sim(\pi,\pi)$ may have low-frequency spectral weight.

The anisotropy of $1/T_1$ generally provides useful information on the wave vector of the spin fluctuations causing the nuclear relaxation. The spin-lattice relaxation is caused by the spin fluctuations perpendicular to the external field [Eq. (8)]. Since the spin-correlation function should be isotropic in cuprates, the anisotropy of $1/T_1$ is determined by the anisotropy of the hyperfine coupling constants $A_\alpha(\mathbf{q})$ and the anisotropy of $A_\alpha(\mathbf{q})$ generally depends on $\mathbf{q}$ if the transferred hyperfine coupling A^1 is sufficiently large.

We have measured the anisotropy of $1/T_1$ at the ladder sites using the center line of high-field NMR with the magnetic field of 8 T along the a, b, and c directions above $T=220$ K, where the relaxation is dominantly magnetic and Eq. (7a) fits the recovery curves well. We obtain

$$(1/T_1)_a:(1/T_1)_b:(1/T_1)c=5.1\pm 0.2:1:4.8\pm 0.2. \tag{19}$$

If the relaxation is caused by the $\mathbf{q}\sim 0$ spin fluctuations, the anisotropy of $1/T_1$ can be obtained from the anisotropy of $A_\alpha(0)$ [Eq. (12)] as

$$(1/T_1)_a:(1/T_1)_b:(1/T_1)c=4.6\pm 0.4:1:4.6\pm 0.4 \tag{20}$$

in reasonable agreement with Eq. (19). Unfortunately, this result is not very conclusive, since it is possible that $\mathbf{A}(\mathbf{Q})$ at $\mathbf{Q}=(\pi,\pi)$ has the same anisotropy as $\mathbf{A}(0)$. In the ladders, one Cu nuclear spin is coupled to three neighboring Cu sites

via 180° Cu-O-Cu bond, therefore, $\mathbf{A}(0)=\mathbf{A}^0+3A^1$ and $\mathbf{A}(\mathbf{Q})=\mathbf{A}^0-3Z^1$. Let us take $A_b^0/(2\hbar\gamma_n)=-24$ T, the value obtained for $CuGeO_3$. Then $\mathbf{A}(0)$ and $\mathbf{A}(\mathbf{Q})$ show the identical anisotropy given by Eq. (12) if the following values are chosen, $A_{ac}^0/(2\hbar\gamma_n)=-2.9$ and $A^1/(2\hbar\gamma_n)=2.8$ T. These values are quite reasonable and there is no reason to rule out such a coincidence. This situation does not allow us to distinguish clearly between $\mathbf{q}\sim 0$ and $\mathbf{q}\sim(\pi,\pi)$ contributions. The comparison of $1/T_1$ at the Cu and the oxygen sites may provide a more decisive answer to this question.

V. SUMMARY

We have clearly identified a distinct Cu NMR/NQR signal from the ladder, the dimer chain, and the ZR singlet chain sites in $Sr_{14}Cu_{24}O_{41}$. Our comprehensive NMR/NQR experiments revealed the following features.

The NMR spectra at the ZR chain sites show a sharp multipeak structure at low temperatures, suggesting a long but periodic superstructure. The structure becomes obscure and peaks merge into a broad single line, indicating thermally induced disorder or motion. A giant oscillation of spin-echo intensity and the τ-dependent NMR spectrum at the dimer chain sites are consistently explained by a strong intradimer exchange and a much weaker interdimer coupling. Models of charge order and dimerization patterns have been proposed, The nuclear spin-lattice relaxation rate $(1/T_1)$ at both the dimer and the ZR chain sites show an activated temperature dependence with a gap of 125 K, consistent with the singlet-triplet splitting of the dimers. Strong frequency dependence of $1/T_1$ at the dimer sites suggests unusually slow spin fluctuations and the localized nature of the triplet excitations. Anomalous increase of $1/T_1$ at the ZR single sites was observed above $T=200$ K.

A clear evidence of motional effects is provided by the quadrupole contribution to $1/T_{1,\mathrm{NQR}}$ at the ladder sites. A pronounced peak in $(1/T_1)_Q$ near $T=100$ K and observed frequency dependence at lower temperatures indicate that the correlation time (τ_c) of the EFG fluctuations changes with temperature. A simple model of motional effects was applied to obtain $1/\tau_c$, which shows an activated temperature dependence with a gap of 230 K. This value, however, is an order of magnitude smaller than the activation gap of electrical conductivity. The magnetic contribution to $1/T_1$ at high temperatures as well as the temperature dependence of K at the ladder sites are consistent with a large spin-gap similar to that observed in the undoped spin-ladder $SrCu_2O_3$. However, insufficient knowledge of the hyperfine coupling constants does not allow us to distinguish whether the dominant weight of the low-frequency spectral weight is located near $\mathbf{q}=0$ or $\mathbf{q}=(\pi,\pi)$.

We conclude the paper by listing questions, which have been raised by the present results and should be addressed by future studies: (1) Microscopic origin of the motion which causes the quadrupole relaxation at the ladder sites. (2) Microscopic origin of the temperature variation of the NMR spectrum, in particular, at the ZR singlet chain sites. (3) Dynamics of the excited triplets of dimer sites. Is it determined by weak interdimer exchange or something else, for example, coupling to the lattice ? (4) Is the magnetic relaxation at the ladder sites described by a Heisenberg ladder model or do the effects of mobile holes need to be considered?

ACKNOWLEDGMENTS

We would like to thank M. Matsuda, G. Shirane, K. Ueda, Z. Fisk, E. Dagotto, and O. Starykh for enlightening discussions and M. Matsuda for kindly providing us with Fig. 1 of the crystal structure. The work at the University of Tokyo was supported by grants for Priority Area and COE research from the Ministry of Education, Science, Sports, and Culture and by a NEDO Grant for International Joint Research.

*Present address: Institute for Solid State Physics, University of Tokyo, Roppongi, Minato-ku, Tokyo 106, Japan

[1] H. J. Schulz, Phys. Rev. B **34**, 6372 (1986); S. Sachdev, *ibid.* **50**, 13 006 (1994); O. A. Starykh, R. R. P. Singh, and A. W. Sandvik, Phys. Rev. Lett. **78**, 539 (1997).

[2] M. Takigawa, N. Motoyama, H. Eisaki, and S. Uchida, Phys. Rev. Lett. **76**, 4612 (1996); M. Takigawa, O. A. Starykh, A. W. Sandvik, and R. R. P. Singh, Phys. Rev. B **56**, 13 681 (1997).

[3] K. M. Kojima, Y. Fudamoto, M. Larkin, G. M. Luke, J. Merrin, B. Nachumi, Y. J. Uemura, N. Motoyama, H. Eisaki, S. Uchida, K. Yamada, Y. Endoh, S. Hosoya, B. J. Sternlieb, and G. Shirane, Phys. Rev. Lett. **78**, 1787 (1997).

[4] For a review, see E. Dagotto and T. M. Rice, Science **271**, 618 (1996).

[5] E. Dagotto, J. Riera, and D. J. Scalapino, Phys. Rev. B **45**, 5744 (1992).

[6] S. R. White, R. M. Noack, and D. J. Scalapino, Phys. Rev. Lett. **73**, 886 (1994).

[7] R. M. Noack, S. R. White, and Scalapino, Phys. Rev. Lett. **73**, 882 (1994).

[8] S. Gopalan, T. M. Rice, and M. Sigrist, Phys. Rev. B **49**, 8901 (1994).

[9] M. Azuma, Z. Hiroi, M. Takano, K. Ishida, and Y. Kitaoka, Phys. Rev. Lett. **73**, 3463 (1994).

[10] R. S. Eccleston, T. Barnes, J. Brody, and J. W. Johnson, Phys. Rev. Lett. **73**, 2626 (1994).

[11] M. Sigrist, T. M. Rice, and F. C. Zhang, Phys. Rev. B **49**, 12 058 (1994).

[12] H. Tsunetsugu, M. Troyer, and T. M. Rice, Phys. Rev. B **49**, 16 078 (1994).

[13] M. Uehara, T. Nagata, J. Akimitsu, H. Takahashi, N. Mori, and K. Kinoshita, J. Phys. Soc. Jpn. **65**, 3474 (1961).

[14] M. W. McElfresh, J. M. D. Coey, P. Strobel, and S. von Molnar, Phys. Rev. B **40**, 825 (1989).

[15] E. M. McCarron III, M. A. Subramanian, J. C. Calabrese, and R. L. Harlow, Mater. Res. Bull. **23**, 1355 (1988).

[16] K. Hirota, D. E. Cox, J. E. Lorenzo, G. Shirane, J. M. Tranquada, M. Hase, K. Uchinokura, H. Kojima, Y. Shibuya, and I. Tanaka, Phys. Rev. Lett. **73**, 736 (1994).

[17] Z. Hiroi, M. Azuma, M. Takano, and Y. Bando, Solid State Chem. **95**, 230 (1991).

[18] N. Motoyama, T. Osafune, T. Kakeshita, H. Eisaki, and S. Uchida, Phys. Rev. B **55**, 3386 (1997).

[19] M. Matsuda and K. Katsumata, Phys. Rev. B **53**, 12 201 (1996).

[20] S. A. Carter, B. Batlogg, R. J. Cava, J. J. Krajewski, W. F. Peck, Jr., and T. M. Rice, Phys. Rev. Lett. **77**, 1378 (1966).
[21] J. Akimitsu, M. Uehara, T. Nagata, S. Matsumoto, Y Kitaoka, H. Takahashi, and N. Mori, Physica C **263**, 475 (1996).
[22] S. Tsuji, K. Kumagai, M. Kato, and Y. Koike, J. Phys. Soc. Jpn. **65**, 3474 (1996).
[23] K. Kumagai, S. Tsuji, M. Kato, and Y. Koike, Phys. Rev. Lett. **78**, 1992 (1997).
[24] M. Matsuda, K. Katsumata, H. Eisaki, N. Motoyama, S. Uchida, S. M. Shapiro, and G. Shirane, Phys. Rev. B **54**, 12 199 (1996).
[25] R. S. Eccleston, M. Azuma, and M. Takano, Phys. Rev. B **53**, R14 721 (1996).
[26] F. C. Zhang and T. M. Rice, Phys. Rev. B **37**, 3759 (1988).
[27] T. Osafune, N. Motoyama, H. Eisaki, and S. Uchida, Phys. Rev. Lett. **78**, 1980 (1997).
[28] M. Kato, K. Shiota, S. Ikeda, Y. Maeno, T. Fujita, and Y. Koike, Physica C **236**, 482 (1996).
[29] A. Abragam, *The Principles of Nuclear Magnetism* (Oxford University Press, Oxford, 1961).
[30] C. P. Slichter, *Principles of Magnetic Resonance* (Springer-Verlag, Berlin, 1989).
[31] A. Narath, Phys. Rev. **162**, 320 (1967).
[32] T. Moriya, Prog. Theor. Phys. **16**, 23 (1956); **16**, 641 (1956).
[33] T. Moriya, Prog. Theor. Phys. **28**, 371 (1962).
[34] C. H. Pennington and C. P. Slichter, Phys. Rev. Lett. **66**, 381 (1991).
[35] M. Takigawa, Phys. Rev. B **49**, 4158 (1994).
[36] K. Ishida, Y. Kitaoka, K. Asayama, M. Azuma, Z. Hiroi, and M. Takano, J. Phys. Soc. Jpn. **63**, 3222 (1994).
[37] M. Itoh, S. Hirashima, and K. Motoya, Phys. Rev. B **52**, 3410 (1995).
[38] M. Troyer, H. Tsunetsugu, and D. Würtz, Phys. Rev. B **50**, 13 515 (1994).
[39] Th. Jolicoeur and O. Golinelli, Phys. Rev. B **50**, 9265 (1994).
[40] S. E. Barrett, D. J. Durand, C. H. Pennington, C. P. Slichter, T. A. Friedmann, J. P. Rice, and D. M. Ginsberg, Phys. Rev. B **41**, 6283 (1990).
[41] The g values for the ladder sites can be estimated as $g_a = 2.0$, $g_b = 2.2$, and $g_c = 2.0$ from the values of K_{orb}. See for example, R. E. Walstedt, R. F. Bell, L. F. Schneemeyer, J. V. Waszczak, and G. P. Espinosa, Phys. Rev. B **45**, 8074 (1992).
[42] M. Takigawa, T. Asano, Y. Ajiro, M. Mekata, and Y. J. Uemura, Phys. Rev. Lett. **76**, 2173 (1996).
[43] T. Shimizu, D. E. MacLaughlin, P. C. Hammel, J. D. Thompson, and S.-W. Cheong, Phys. Rev. B **52**, R9835 (1995).
[44] S. Sachdev and K. Damle, Phys. Rev. Lett. **78**, 943 (1997).
[45] J. Kishine and H. Fukuyama, J. Phys. Soc. Jpn. **66**, 23 (1997).
[46] N. Bloembergen, E. M. Purcell, and R. V. Pound, Phys. Rev. **73**, 679 (1948).
[47] K. Ishida, Y. Kitaoka, Y. Tokunaga, S. Matsumoto, K. Asayama, M. Azuma, Z. Hiroi, and M. Takano, Phys. Rev. B **53**, 2827 (1996).
[48] A. W. Sandvik, E. Dagotto, and D. J. Scalapino, Phys. Rev. B **53**, R2934 (1996).
[49] We used the values $g_a = 2.05$, $g_b = 2.26$, and $g_c = 2.04$ determined by ESR in Ref. 19.
[50] F. Mila and T. M. Rice, Physica C **157**, 561 (1989).
[51] M. Itoh, M. Sugahara, T. Yamauchi, and Y. Ueda, Phys. Rev. B **53**, 11 606 (1996).
[52] Y. Fagot-Revurat, M. Horvatić, C. Berthier, J. P. Boucher, P. Ségransan, G. Dhalenne, and A. Revcolevschi, Phys. Rev. B **55**, 2964 (1997).
[53] E. L. Hahn and D. E. Maxwell, Phys. Rev. **88**, 1070 (1952); see also p. 497 of Ref. 29.
[54] We thank Z. Fisk for bringing this point to our attention.
[55] Although our simple model predicts an equal intensity for all four lines at point a, transverse coupling that leads to the mutual spin flip will cause the inner two lines to decay faster than the outer two lines at large τ. This may account for the suppression of the inner region even for the spectrum at point a.
[56] Z. Hiroi, S. Amelinckx, G. Van Tendeloo, and N. Kobayashi, Phys. Rev. B **54**, 15 894 (1996).
[57] K. Ueda (private communication).
[58] M. Takigawa and G. Saito, J. Phys. Soc. Jpn. **55**, 1233 (1986).